Macrophage innate immune gene expression requires dynamic regulation of the nuclear paraspeckle

Sikandar Azam[1], Kaitlyn S. Armijo[1], Chi G. Weindel[1], Alice Devigne[2], Shinichi Nakagawa[3], Tetsuro Hirose[4], Susan Carpenter[2], Robert O. Watson[1], Kristin L. Patrick[1]*

[1]Department of Microbial Pathogenesis and Immunology, Texas A&M University, School of Medicine, Bryan, TX 77807 USA.

[2]Department of Molecular, Cell, & Developmental Biology, University of California, Santa Cruz, Santa Cruz, CA 95064 USA.

[3]RNA Biology Laboratory, Hokkaido University, Sapporo 060-0812 Japan.

[4]RNA Biofunction Laboratory, Graduate School of Frontier Biosciences, Osaka University, Osaka 565-0871 Japan.

*corresponding author: kpatrick03@tamu.edu

ABSTRACT

There is a growing appreciation for membraneless organelles (MLOs) in regulating cellular stress responses. Here, we demonstrate a role for the nuclear paraspeckle, a highly ordered biomolecular condensate that nucleates on the *Neat1* lncRNA, in both activating and repressing innate immune gene expression in murine macrophages. In response to a variety of innate agonists, macrophages rapidly upregulate and then downregulate paraspeckles. Paraspeckle maintenance and aggregation requires active transcription and MAPK signaling. Downregulation of paraspeckles, an adaptation seemingly unique to macrophages, is mediated by the nuclear RNA exosome, via degradation of *Neat1*. Primary macrophages lacking *Neat1* (*Neat1* KO) misregulate many critical inflammatory cytokines, with a failure to upregulate genes like *Il6* and *Cxcl9* and to downregulate others (e.g., *Csf3* and *Vegfa*), at the transcript and protein levels in response to lipopolysaccharide (LPS) treatment. We propose that dynamic assembly and disassembly of paraspeckles help macrophages mount an innate immune response by controlling the availability of RNA processing machineries in the nucleus. Collectively, these data argue that stress-responsive biomolecular condensates play a prominent role in modulating immune cell function.

INTRODUCTION

Biologists have long been interested in the functions of the membrane-bound organelles that define eukaryotic cells. More recently, membrane*less* organelles (MLO) have captured the attention of many. MLOs are biomolecular condensates that form through the process of liquid-liquid phase separation (LLPS). MLOs compartmentalize a variety of cellular processes in both the cytosol and the nucleus. The nucleus houses several MLOs, including the nucleolus, Cajal bodies, PML nuclear bodies, nuclear speckles, and nuclear paraspeckles. By sequestering both RNAs and proteins, nuclear condensates regulate many steps in gene expression, including transcription, pre-mRNA splicing, RNA editing, and mRNA export. A common theme of MLOs is their ability to change number, size, structure, and composition in response to cellular stress (1, 2). While phenomena related to condensate assembly have been extensively described, mechanistic links between MLO dynamics and the function of these domains in cellular homeostasis remain poorly understood.

One nuclear condensate with well-established links to stress responses is the nuclear paraspeckle (3-5). Discovered in HeLa cells in 2002, nuclear paraspeckles were first defined as nuclear domains enriched for paraspeckle protein 1 (PSP1) found in proximity to SC35-containing nuclear speckles (4). Paraspeckles are characterized by their spheroidal shape and distinct core and shell-like structure (4, 6, 7). These highly ordered MLOs organize on a long lncRNA called nuclear paraspeckle assembly transcript 1 (*Neat1*) (7). The *Neat1* gene encodes two isoforms, *Neat1_1* and *Neat1_2*. While both are found in paraspeckles, only *Neat1_2*, the long isoform (22.7 kb in humans, 21.2 kb in mice), is required for paraspeckle assembly. Although the two isoforms share the same promoter, their processing is distinct; instead of being polyadenylated, the 3' end of *Neat1_2* is stabilized by an atypical triple helix structure (5, 8). *Neat1_1*, on the other hand, is spliced and polyadenylated (7, 9).

Paraspeckles are comprised of ~50 copies of *Neat1_2* and a cohort of RNA binding proteins RBPs), several of which are required for paraspeckle assembly/maintenance. The current list of eight essential paraspeckle proteins includes: splicing factor proline- and glutamine-rich protein (SFPQ), the non-POU domain-containing octamer-binding protein (NONO), found in sarcoma (FUS), RNA binding protein 14 (RBM14), the Brahma-related gene-1 (BRG1), DAZ-associated protein 1 (DAZAP1), and two heterogeneous nuclear ribonucleoproteins, HNRNPK and HNRNPH3 (7, 10). Other proteins like PSPC1 are enriched in PS but not required for their assembly (11).

Paraspeckles form co-transcriptionally. First, SFPQ and NONO load onto the nascent *Neat1*_2 transcript as it is being made, forming an intermediate *Neat1*_2 ribonucleoprotein. Then,

FUS and RBM14 are recruited to drive the formation of mature paraspeckles (3, 7, 12). Paraspeckle-associated RBPs like SFPQ, NONO, FUS, RBM14, HNRNPK, etc. have been implicated in processes like transcription, splicing, and polyadenylation. As proteins are incorporated into growing PSs, their ability to participate in other nuclear gene expression pathways is altered. This sequestration mechanism has been proposed for SFPQ-mediated transcription of the RNA editing ADARB2 gene (13) and TDP-43 control of alternative polyadenylation (14). Likewise, association of the SWI/SNF complex protein ARID1B with the PS has been shown to influence alternative splicing in HEK293T cells (15).

Because of links between *Neat1* and cancer, neurodegenerative disease, and inflammatory disorders, there is growing interest in how *Neat1* and paraspeckles control cellular homeostasis (16, 17). Specialized cell types, like neurons and immune cells, are constantly receiving and responding to environmental inputs that trigger remarkable changes to their transcriptomes and proteomes. Innate immune cells like macrophages are particularly exemplary of this behavior. Macrophages, our body's first line of defense against foreign agents, express a panoply of pattern recognition receptors that allow them to sense pathogen- and damage-associated molecular patterns (PAMPs and DAMPs). When these sensors are engaged, they trigger a series of complex signal transduction cascades, which activate transcription factors to turn on *de novo* expression of cytokines, chemokines, and antimicrobial mediators. Several studies have begun to link PSs to innate immune gene expression and antiviral responses. *Neat1*-deficient mice mount reduced inflammatory responses during models of peritonitis and pneumonia (18) and *Neat1* itself can be upregulated in response to DNA or RNA viral infection in some cell types. Depletion of *Neat1* has been shown to promote expression of inflammatory genes like IL-8 via sequestration of repressive SFPQ from the IL-8 promoter (19) and has been linked to reduced dengue virus replication (20). Despite these intriguing links between PSs and inflammation, it remains to be seen how PSs functions in a *bona fide* immune cells like macrophages.

We hypothesized that nuclear MLOs like PSs help the nucleus regulate transcription of innate immune genes in response to pathogen sensing. Consistent with a role for these MLOs in sensing and responding to pathogens, we found that paraspeckles undergo rapid dynamic changes in macrophages following several innate stimuli. Notably, we observed that PS aggregate almost immediately upon pattern recognition receptor engagement and disappear at 2h post-stimulation of TLR4, TLR2, or cGAS. We report that PS upregulation in macrophages requires active transcription and disassembly of PSs and loss of *Neat1* RNA is dependent on the nuclear RNA exosome. In the absence of *Neat1*, immortalized bone marrow derived macrophages (iBMDMs) and primary BMDMs fail to fully induce expression of inflammatory genes that are

upregulated as part of the innate response and fail to limit expression of genes that are downregulated upon LPS treatment, highlighting a critical role for *Neat1* and the PS in helping macrophages mount a balanced innate immune gene expression program.

RESULTS

Paraspeckles are rapidly up- and down-regulated in response to innate agonist treatment of macrophages

To begin to define the dynamics of paraspeckle formation during macrophage activation, we employed a technique to simultaneously detect the *Neat1* lncRNA by RNA-FISH and paraspeckle proteins like PSP1 by immunofluorescence (FISH-IF). Our FISH probes only anneal to sequences in the paraspeckle-forming *Neat1_2* lncRNA (which we will refer to as *Neat1* from now on). Using FISH-IF for *Neat1* and PSP1, we observed that resting RAW 264.7 macrophages maintain two clear PSs, consistent with previous reports demonstrating co-transcriptional paraspeckle formation at each *Neat1* genomic locus (21, 22). We then treated macrophages with lipopolysaccharide (LPS) (100 ng/ml) and performed FISH-IF over a time-course of treatment. LPS, a component of the outer membrane of gram-negative bacteria, stimulates expression of hundreds of innate immune genes (e.g., *Tnf* and *Il1b* by engaging TLR4 and activating transcription factors like NFκB and IRF3 (**Fig. S1A**). At 30 minutes post-LPS treatment, we observed a dramatic upregulation of paraspeckles in RAW 264.7 macrophages (**Fig. 1A**). At 60 minutes, paraspeckle area remained high, but qualitatively, PSs became more dispersed throughout the nucleus. This was concomitant with an approximately 2- to 3-fold increase in total *Neat1* RNA as measured by RT-qPCR (**Fig. 1B**; primers designed to amplify a region unique to the long *Neat1_2* isoform). At 120 min post-LPS, PS signal was virtually undetectable, with no observable *Neat1* or PSP1 puncta. This was concomitant with a loss of *Neat1* RNA signal by RT-qPCR (**Fig. 1B**). By 240 minutes post-LPS, paraspeckles started to reform although total *Neat1* RNA remained low. At 6h post-LPS, cells were heterogeneous in their PS numbers, with most cells having 0, 1, or 2 paraspeckle and about 20% of cells maintaining higher numbers (**Fig. S1B**). By 8h post-LPS, the percentage of cells maintaining >2 paraspeckles increased to ~50%, suggestive of cells restarting the cycle of PS aggregation (**Fig. S1C**). Another abundant lncRNA, *Malat1*, which is encoded in the genome directly downstream of *Neat1,* showed no evidence of up or downregulation over the course of an 8h LPS treatment (**Fig. S1D**). We observed similar paraspeckle dynamics in primary BMDMs (**Fig. 1C**), with paraspeckle area peaking at 30 minutes post-LPS and signal ablation at 120 minutes post-LPS. Compared to other cell

Figure 1

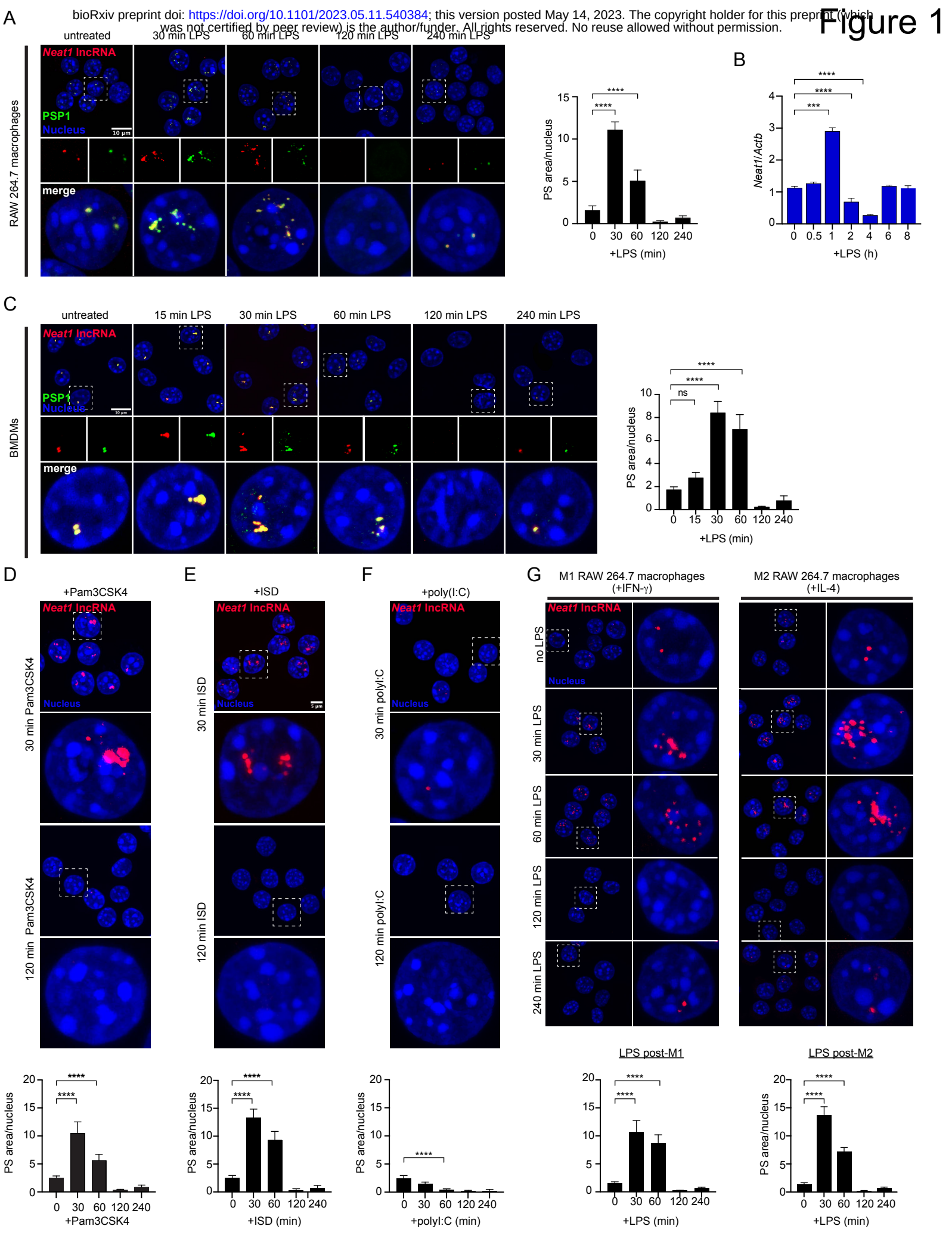

Figure 1: Nuclear paraspeckles are dynamically regulated following innate immune agonist treatment of macrophages

(A) RNA-FISH of *Neat1* (red) and immunofluorescence microscopy of PSP1 (green) in RAW 264.7 macrophages after LPS treatment (100ng/ml). Quantitation of paraspeckle area/nucleus on right.
(B) RT-qPCR of *Neat1_2* transcript levels in RAW 264.7 macrophages after LPS treatment (100ng/ml) shown relative to *Actb.*
(C) As in (A) but with BMDMs treated with 10ng/ml LPS. Quantitation of paraspeckle area/nucleus on right.
(D) RNA-FISH of *Neat1* (red) in RAW 264.7 macrophages after Pam3CSK4 treatment (100ng/ml). Quantitation of paraspeckle area/nucleus below.
(E) As in (D) but with dsDNA transfection (ISD) (1μg/ml).
(F) As in (D) but with dsRNA transfection (polyI:C) (500ng/ml)
(G) RNA-FISH of *Neat1* and PSP1 in RAW 264.7 macrophages after LPS treatment (100ng/ml) following overnight polarization into M1- (+IFN-γ; 50ng/ml) or M2 (+IL-4; 25ng/ml)-like macrophages. Quantitation of paraspeckle area/nucleus below.

Statistical tests: Data is presented as the mean of three biological replicates unless otherwise noted with error bars representing SEM. At least 100 cells were counted over multiple coverslips per condition. Statistical significance was determined using a one-way ANOVA. ***p<0.001, ****p<0.0001.

Figure S1

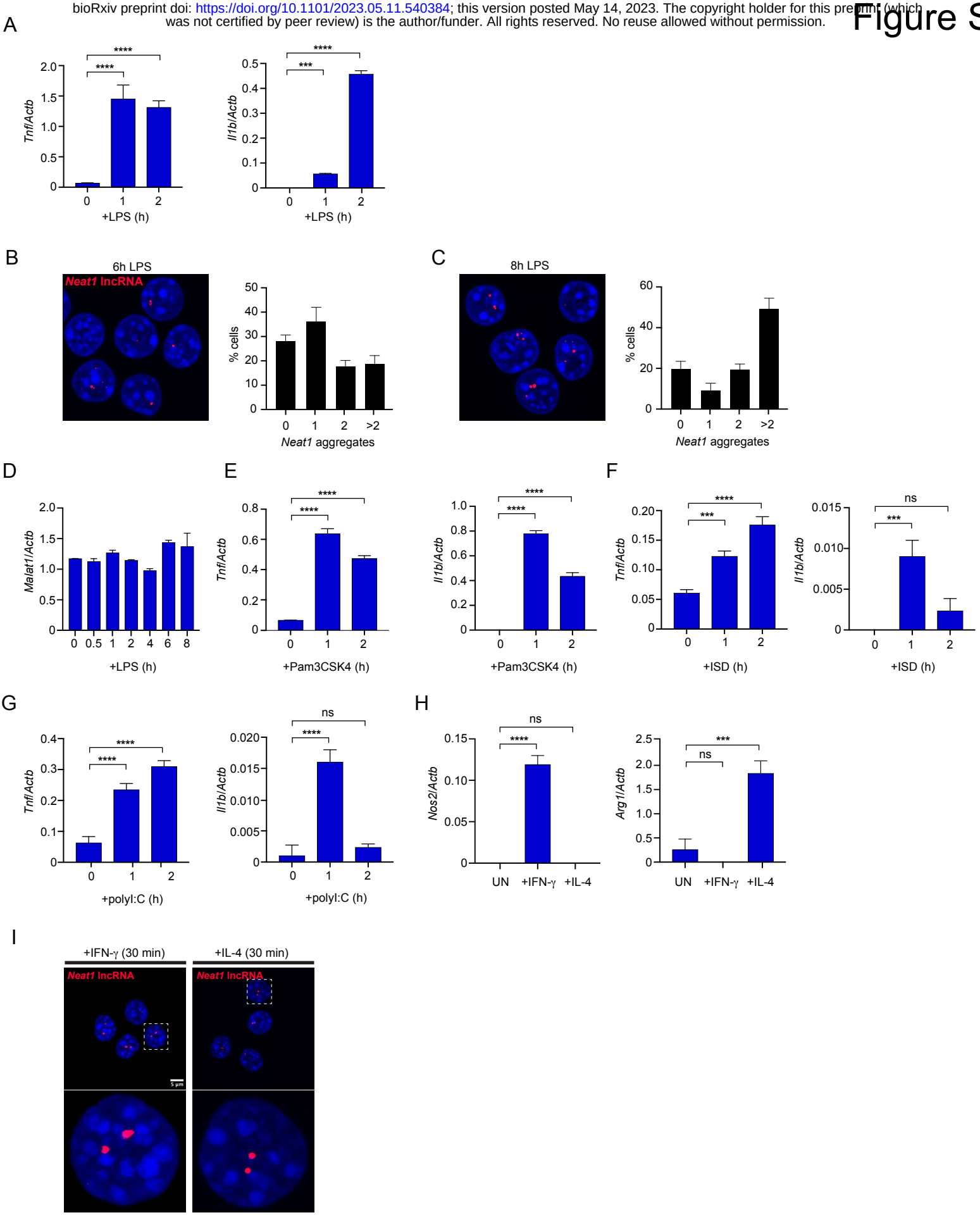

Figure S1: Supplementary Data for Figure 1

(A) RT-qPCR of *Tnfa* and *Il1b* transcript levels in RAW 264.7 macrophages after LPS treatment, (100ng/ml) shown relative to *Actb.*
(B) RNA-FISH of *Neat1* (red) in RAW 264.7 macrophages at 6h post-LPS (100ng/ml) treatment. To quantify on right, cells with different numbers of *Neat1* aggregates were manually counted (n>100) and binned into cells with 0, 1, 2, and >2 paraspeckles.
(C) As in (B) but at 8h post LPS-stimulation
(D) RT-qPCR of *Malat1* transcript levels in RAW 264.7 macrophages after LPS treatment (100ng/ml) shown relative to *Actb.*
(E) As in (A) but after Pam3CSK4 (100ng/ml) treatment
(F) As in (A) but after dsDNA (ISD) (1μg/ml) transfection
(G) As in (A) but after dsRNA (polyI:C) (500ng/ml) transfection.
(H) RT-qPCR of M1- (*Nos2*) and M2-characteristic (*Arg1*) transcripts 24h post IFN-γ (50 ng/ml) or IL-4 (25 ng/ml) treatment, shown relative to *Actb*
(I) RNA-FISH of *Neat1* (red) in RAW 264.7 macrophages at 24h post-M1 and M2 polarization as in (H).

Statistical tests: Data is presented as the mean of three biological replicates unless otherwise noted with error bars representing SEM. At least 100 cells were counted over multiple coverslips per condition. Statistical significance was determined using a one-way ANOVA. *p<0.05, **p<0.01, ***p<0.001, ****p<0.0001.

types, the kinetics of paraspeckle induction in macrophages is faster (30 minutes v. 48h post-Hepatitis Delta virus infection of HEK293Ts (23)). To the best of our knowledge, the phenomena of paraspeckle disassembly and recovery that we report at 2h and 4h post-LPS treatment has not been reported as part of normal cellular responses in other mammalian cell types, and thus might represent a macrophage-specific adaptation.

We next asked whether paraspeckle dynamics triggered by LPS, which activates pathogen sensing cascades via TLR4, were unique. Having seen very similar paraspeckle dynamics between RAW 264.7 macrophages cells and primary BMDMs, we chose to continue studies with the genetically tractable RAW 264.7 cell line. Likewise, having seen identical patterns for the *Neat1* lncRNA by FISH and the PSP1 protein by IF across multiple experiments, we opted to track PS by virtue of *Neat1* FISH alone. We treated RAW 264.7 macrophages with a panel of innate immune agonists and measured PS formation by RNA-FISH. Treatment of cells with the TLR2 agonist Pam3CSK4 (**Fig. 1D**; **Fig. S1E**) or the cGAS agonist cytosolic dsDNA (ISD) (**Fig. 1E**; **Fig. S1F**) triggered PS dynamics that closely followed those induced by LPS. Surprisingly, transfection of polyI:C, a dsRNA agonist of TLR3 (endosomal) and RIG-I/MDA5 (cytosolic) RNA sensing cascades, rapidly ablated *Neat1* signal in the nucleus (**Fig. 1F**; **Fig. S1G**). Our polyI:C results contrast a previous report that showed PS upregulation in HeLa cells post-polyI:C transfection (24), further arguing that that macrophages regulate paraspeckles in a fundamentally different way than non-immune cells.

Macrophage polarization is an important determinant in dictating innate immune outcomes (25). Macrophages can take on a classical pro-inflammatory M1 state when treated with IFN-γ or can be alternatively activated to a wound healing M2 state after treatment with IL-4. To determine whether macrophage polarization impacts PS dynamics, we treated RAW 264.7 macrophages overnight with IFN-γ (M1) or IL-4 (M2). We confirmed polarization by measuring canonical M1/M2 transcripts by RT-qPCR (**Fig. S1H**). We did not see dramatic upregulation of PS at 30min or 24h post-IFN- γ or IL-4 treatment alone, suggesting that treatment with these cytokines is not sufficient to upregulate PSs (**Fig. S1I**). We then repeated our LPS time-course in these M1 or M2 macrophages. In both cases, we qualitatively observed hyper-accumulation of *Neat1* by RNA-FISH at 30 and 60 min, suggesting that polarized macrophages are primed to upregulate PS (**Fig. 1G**). Downregulation of PS occurred with similar kinetics in M1 and M2-polarized macrophages (**Fig. 1G**). Together, these data identify nuclear PSs as immune-responsive MLOs in macrophages that are dynamically regulated downstream of multiple innate sensing cascades.

Paraspeckle upregulation in macrophages can sequester nuclear RNA binding proteins

Paraspeckles contain many copies of the *Neat1* RNA and an array of RNA binding proteins (26). We next asked whether co-localization between *Neat1* and core paraspeckle proteins is concomitant with *Neat1* upregulation and whether the composition of paraspeckle in a specialized cell type like the macrophage resembles that which has been reported in other cell types. In resting and LPS-treated RAW 264.7 macrophages, we observed the highest degree of colocalization between *Neat1* and PSP1 (**Fig. 2A**) and SFPQ (**Fig. 2B**). Some colocalization between NONO and *Neat1* was observed at baseline, and this increased upon LPS treatment (**Fig. 2C**). We found that total cellular levels of these paraspeckle proteins remain constant over a 60 min time-course of LPS treatment, supporting model whereby already synthesized paraspeckle proteins in the nucleus are brought into paraspeckles as they grow (**Fig. S2A**). Surprisingly, PS proteins deemed essential in other cell types, e.g., FUS and BRG1, displayed no evidence of punctate staining reminiscent of paraspeckles at any time-point post-LPS treatment, which brings into question the relevance of these proteins in the macrophage paraspeckle (**Fig. S2B-C**).

In addition to these “core” paraspeckle proteins, 20+ additional RNA binding proteins involved in a variety of nuclear processes (pre-mRNA splicing, RNA editing, mRNA export, etc.) have been shown to localize to and/or purify with the paraspeckle (27). We posited that aggregation of paraspeckles in macrophages following innate stimuli could function to sequester RBPs from, or release RBPs into, the nucleoplasm. To begin to test this hypothesis, we took a candidate approach. One RBP with reported association with paraspeckle proteins and links to innate immune gene expression is the splicing factor hnRNP M, which represses intron removal of inflammatory cytokines like *Il6* (28). By FISH-IF, we saw a marked increase in colocalization between hnRNP M and *Neat1* at 30 minutes post-LPS treatment (**Fig. 2D**). Components of the SWI/SNF nucleosome remodeling complex, which play an important role in activating expression of secondary response genes like *Il6* have also been found in paraspeckles in other model cell types (29). In resting macrophages, we found that the SWI/SNF protein BRM aggregates into striking nuclear bodies, but these did not colocalize with *Neat1* (**Fig. 2E**). Only modest colocalization was measured between BRM and *Neat1* after LPS treatment. These data begin to suggest that paraspeckle composition in macrophages is different from that in other cell types.

We finally asked whether paraspeckles sequester innate immune transcription factors that are activated downstream of pattern recognition receptors like TLR4. Overall, colocalization between *Neat1* and the two factors queried, NFκB and STAT1, was very low (**Fig. 2F-G**). We did measure a slight, but statistically significant, increase in colocalization between *Neat1* and

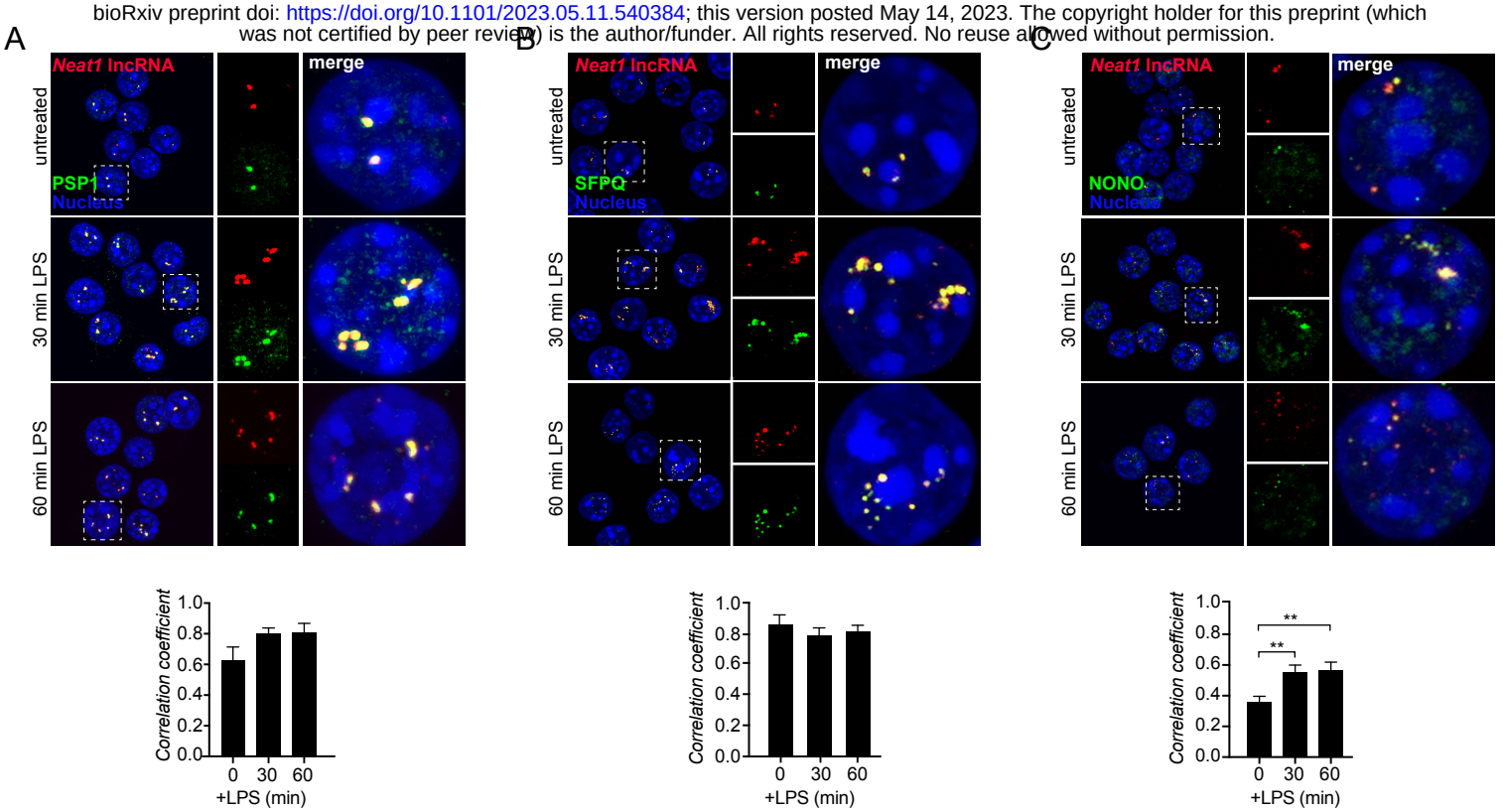

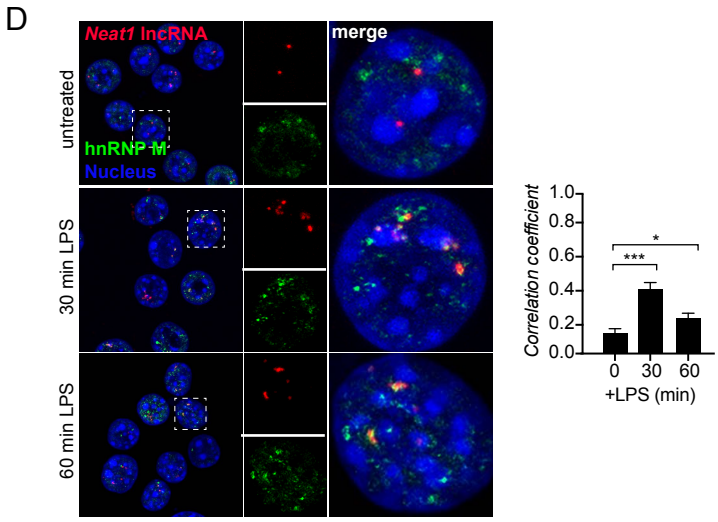

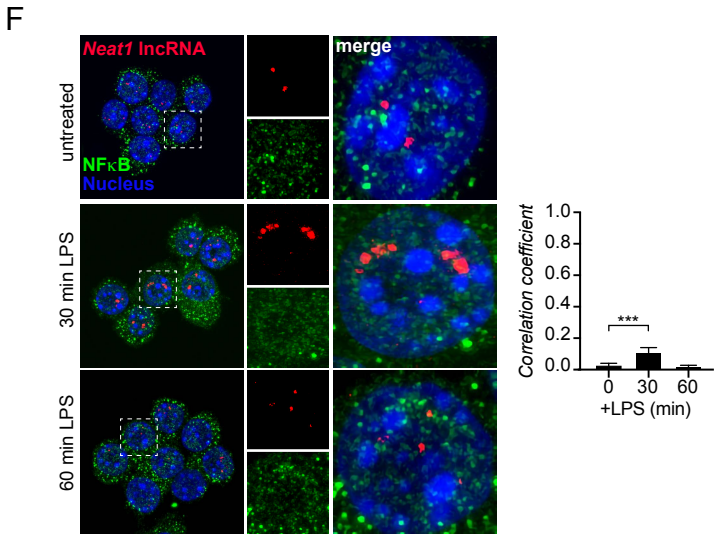

Figure 2

Figure 2: Paraspeckle upregulation in macrophages sequesters nuclear RNA binding proteins.

(A) RNA-FISH of *Neat1* (red) and immunofluorescence microscopy of PSP1 (green) in RAW 264.7 macrophages at 30 and 60 minutes post-LPS treatment (100ng/ml). Correlation coefficient between *Neat1* and PSP1 quantified below.
(B) As in (A) but for SFPQ.
(C) As in (A) but for NONO.
(D) As in (A) but for hnRNP M
(E) As in (A) but for BRM
(F) As in (A) but for NFκB (RelA/p65)
(G) As in (A) but for STAT1

Statistical tests: Data is presented as the mean of three biological replicates unless otherwise noted with error bars representing SEM. At least 100 cells were counted over multiple coverslips per condition. Colocalization coefficient was measured using the ImageJ plugin Coloc2. Statistical significance was determined using a one-way ANOVA. *p<0.05, **p<0.01, ***p<0.001.

A

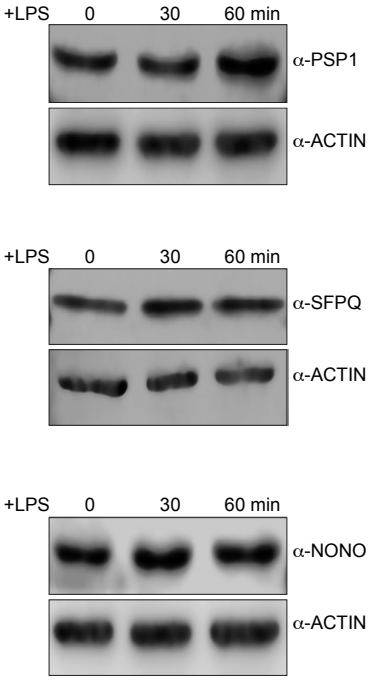

B

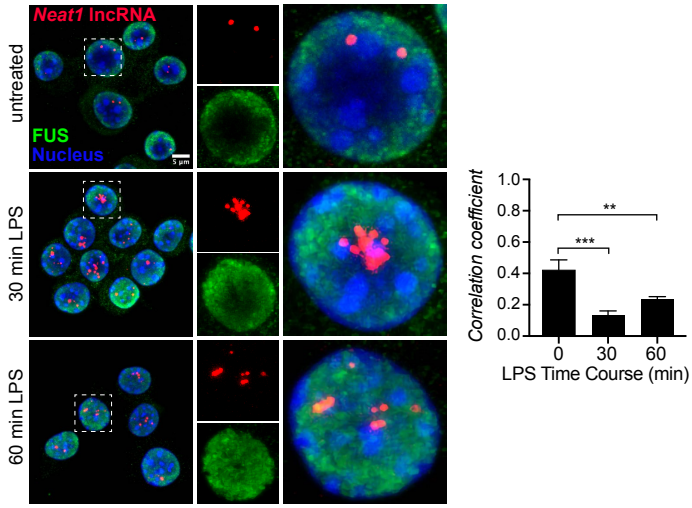

C

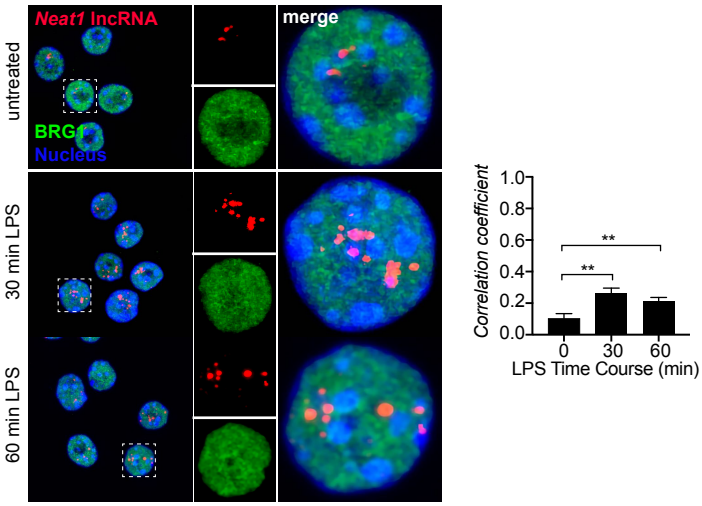

Figure S2

Figure S2: Supplementary Data for Figure 2

(A) Immunoblot analysis of PSP1, SFPQ, and NONO in RAW 264.7 macrophages after LPS (100ng/ml) stimulation. Beta actin used as a loading control. Representative blot of n=3.
(B) RNA-FISH of *Neat1* (red) and immunofluorescence microscopy of FUS (green) in RAW 264.7 macrophages at 30 and 60 min post-LPS treatment (100 ng/ml). Correlation coefficient between *Neat1* and FUS quantified to the right.
(C) As in (B) but for BRG1.

Statistical tests: Data is presented as the mean of three biological replicates unless otherwise noted with error bars representing SEM. At least 100 cells were counted over multiple coverslips per condition. Colocalization coefficient was measured using the ImageJ plugin Coloc2. Statistical significance was determined using a one-way ANOVA. **p<0.01, ***p<0.001.

these transcription factors post LPS-stimulation, particularly for NFκB (**Fig. 2F**). This could represent enrichment of NFκB at the site of *Neat1* transcription and would be consistent with ChIP-seq experiments that show enrichment of the NFκB subunit RelA at the *Neat1* promoter in response to LPS (**Fig. S3D**). Together, these data hint at compositional differences between macrophage paraspeckles and those previously described in other model cell types. They also suggest that RBPs previously linked to post-transcriptional regulation of innate immune gene expression (e.g., hnRNP M) have links to the paraspeckle in macrophages.

Transcription and MAPK signaling are required to maintain and upregulate paraspeckles in macrophages

Given the rapid up- and downregulation of paraspeckles over the 4h LPS-time course queried, we set out to investigate the cellular pathways that control PS maintenance and aggregation in macrophages. First, we asked whether transcription was required for PS upregulation after LPS treatment. Briefly, RAW 264.7 macrophages were treated with the transcription inhibitor actinomycin D (ActD) for 30 minutes and *Neat1* was monitored by FISH and RT-qPCR 30 min post-LPS. Treatment with ActD not only prevented LPS-induced paraspeckle upregulation, it inhibited paraspeckle maintenance all together, as we could no longer detect *Neat1* puncta in resting macrophages after 30 min of ActD (**Fig. 3A**). Curiously, this loss of paraspeckle signal did not correspond directly with total cellular levels of *Neat1* lncRNA, which remained high for at least 60 min after ActD (**Fig. 3B**) and ActD/LPS treatment (**Fig. 3C**). This suggests that while active transcription is needed to maintain and aggregate paraspeckles, this is likely due more to reliance on the act of transcription for assembling paraspeckles, rather than a need to synthesize new *Neat1*. The kinetics of *Neat1* lncRNA turnover after transcription shut off were on the order of 120 minutes in RAW 264.7 macrophages (**Fig. 3B-C; Fig. S3A**)—the same time-point at which we see loss of paraspeckles after LPS treatment (**Fig. 1A**). Degradation of the *Neat1* RNA after transcriptional shut-off far exceeded that of a stable housekeeping gene like *Gapdh* (**Fig. 3D**; **Fig. S3B**) and was even faster than that of another previously identified short lived non-coding RNA, *Kcnq10t1* (30) (**Fig. 3E**; **Fig. S3C**), consistent with earlier reports of *Neat1* being an unstable/short-lived RNA (30). Together, these data argue that *de novo* transcription is required both to maintain paraspeckles in macrophages, as reported in (22), and to upregulate paraspeckles upon LPS treatment.

We next sought to identify the signaling cascades that promote *Neat1* transcription and upregulation upon LPS treatment. LPS stimulation of TLR4, and TLR signaling in general, activate a complex network of kinase cascades, including MEK, JNK, and p38 MAP kinases, AKT

Figure 3

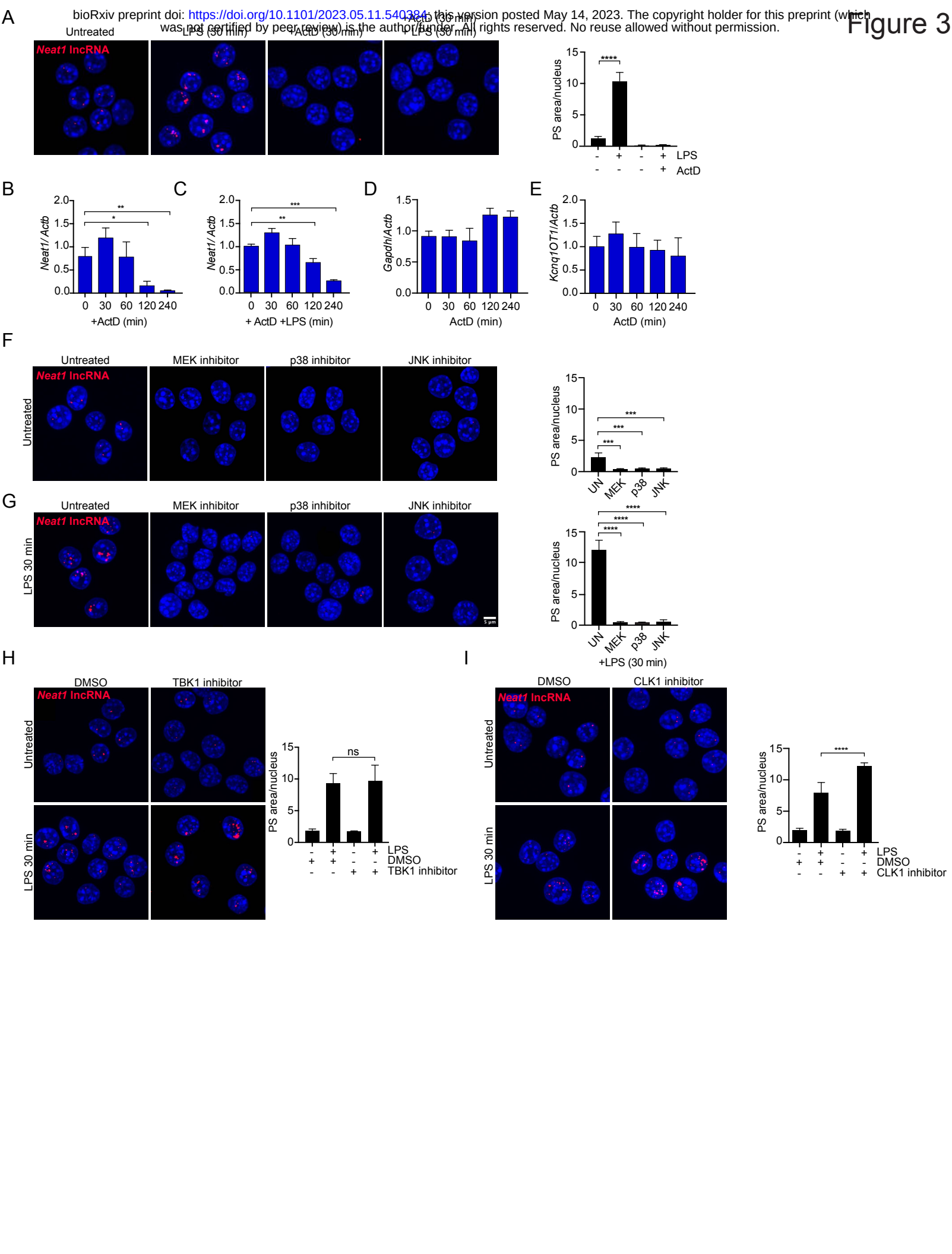

Figure 3: De novo transcription and basal MAPK signaling maintain PSs in macrophages.

(A) RNA-FISH of *Neat1* (red) in RAW 264.7 macrophages after actinomycin D treatment (ActD) (5μg/ml) followed by LPS stimulation for timepoints indicated. Quantitation of paraspeckle area/nucleus on right.
(B) RT-qPCR of *Neat1_2* transcript levels in RAW 264.7 macrophages after ActD treatment, (5μg/ml) shown relative to *Actb*.
(C) As in (B) but with LPS (100ng/ml) treatment following 30 min ActD.
(D) As in (B) but for *Gapdh*
(E) As in (B) but for *Kcnq1OT1*
(F) RNA-FISH of *Neat1* (red) in RAW 264.7 macrophages after MAPK inhibitor treatment (Add concentrations for each) for 45 minutes. Quantitation of paraspeckle area/nucleus on right.
(G) As in (F) but with the addition of LPS (100ng/ml) for 30 min, following ActD. Quantitation of paraspeckle area/nucleus on right.
(H) RNA-FISH of *Neat1* (red) in RAW 264.7 macrophages after treatment with the TBK1 inhibitor (GSK-8612; 10μM) at 0 and 30 minutes post-LPS stimulation. Quantitation of paraspeckle area/nucleus on right.
(I) As in (H) but with CLK1 inhibitor (Cpd 23; 10μM). Quantitation of paraspeckle area/nucleus on right.

Statistical tests: Data is presented as the mean of three biological replicates unless otherwise noted with error bars representing SEM. At least 100 cells were counted over multiple coverslips per condition. Statistical significance was determined using a one-way ANOVA. *p<0.05, **p<0.01, ***p<0.001, ****p<0.0001.

A

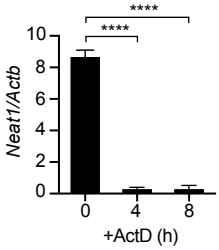

B

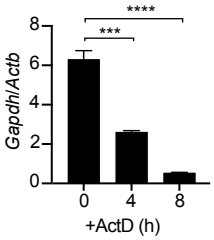

C

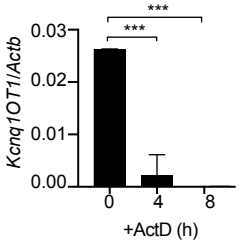

D

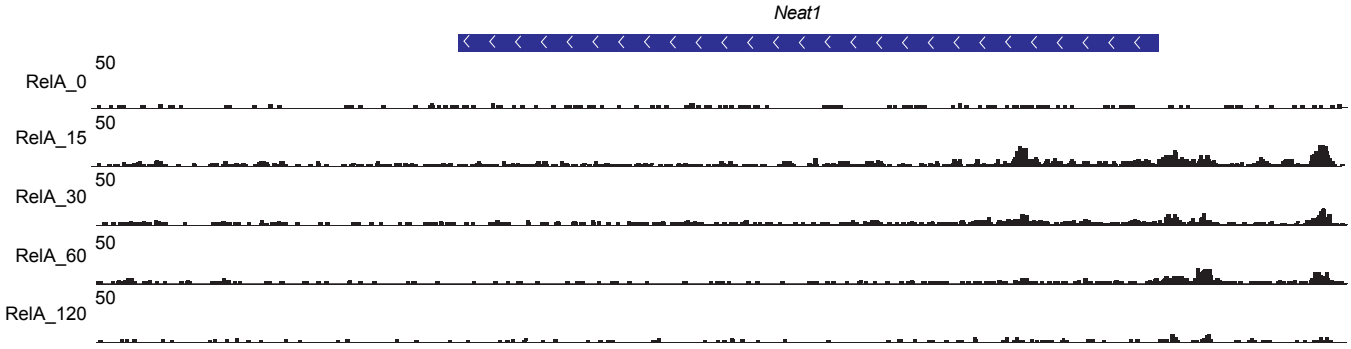

E

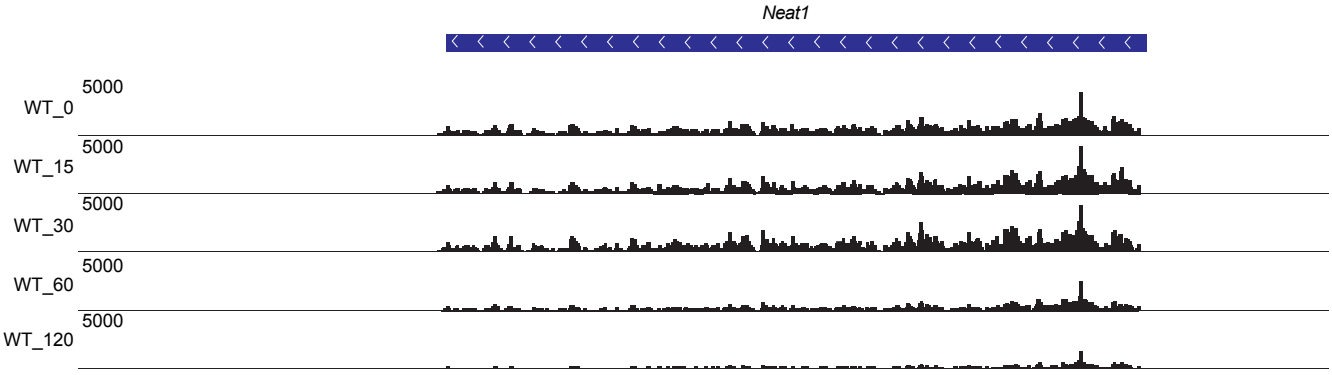

Adapted from Tong et al., 2016

F

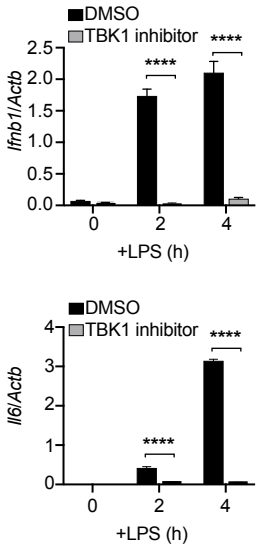

G

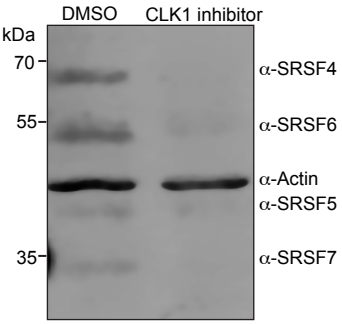

Figure S3: Supplementary Data for Figure 3

(A) RT-qPCR of *Neat1_2* transcript levels in RAW 264.7 macrophages after 4h and 8h ActD treatment, (5μg/ml) shown relative to *Actb*.
(B) As in (B) but for *Gapdh*
(C) As in (B) but for *Kcnq1OT1*
(D) IGV tracks of ChIP-seq data for RelA (NFκB subunit) at the *Neat1* promoter over a 120 minute time course of LPS treatment. From Tong et al., 2016. GEO Accession numbers: GSM1645112 (RelA_0), GSM1645114 (RelA_15), GSM1645116 (RelA_30), GSM1645118 (RelA_60), GSM1645120 (RelA_120).
(E) IGV tracks of RNA-seq reads at *Neat1* over a 120min time course of LPS treatment. From Tong et al., 2016. GEO Accession numbers: GSM1645338 (WT_0), GSM1645340 (WT_15), GSM1645342 (WT_30), GSM1645344 (WT_60), GSM16453346 (WT_120).
(F) RT-qPCR of *Ifnb1* and *Il6* transcript levels in LPS-treated RAW 264.7 macrophages +/- the TBK1 inhibitor (GSK-8612; 10μM).
(G) Immunoblot analysis of phosphorylated SR proteins in RAW 264.7 macrophages +/- treatment with the CLK1 inhibitor (Cpd 23; 10μM).

Statistical tests: Data is presented as the mean of three biological replicates unless otherwise noted with error bars representing SEM. Statistical significance was determined using a one-way ANOVA. ***p<0.001, ****p<0.0001.

and PI3-K, IκB kinase, and the noncanonical IκB kinase homologs IKK-ε and TBK1 (31, 32). To begin to test the role of MAPKs in regulating PS dynamics in macrophages, we LPS-treated RAW 264.7 macrophages for 30 min following pretreatment for 45 minutes with a MEK inhibitor (U0126), a JNK inhibitor (SP600125), or a p38 inhibitor (SB203580). Remarkably, not only did we see paraspeckles fail to accumulate after all three MAPK inhibitor treatments, but we saw loss of paraspeckles in untreated macrophages, suggesting that basal MAPK signaling is important for maintaining paraspeckles in resting cells (**Fig. 3F-G**). Inhibiting other potentially relevant cellular kinases like TBK1 (**Fig. 3H, S3F**), which is activated downstream of TLR4 to phosphorylate the transcription factor IRF3, or CLK1, which is activated downstream of AKT signaling to regulate phosphorylation of SR proteins (33, 34), did not ablate paraspeckles (**Fig. 3I-S3G**). In fact, treatment with the CLK1 inhibitor resulted in modest hyperaggregation of *Neat1* at 30 minutes post-LPS treatment. These results implicate MAPKs as positive regulators of paraspeckle maintenance and hint at SR protein phosphorylation negatively regulating paraspeckle aggregation in macrophages.

The *Neat1* lncRNA is targeted to the nuclear exosome by the NEXT complex to regulate PS dynamics in macrophages

In the nucleus, RNA turnover is controlled by the RNA exosome, a multiprotein complex responsible for 3' end processing and/or degradation of various types of RNAs (35). The exosome forms a barrel structure and has two associated 3' to 5' exoribonucleases: EXOSC10/RRP6 and DIS3 (**Fig. 4A**). RNAs are targeted to the exosome for processing or degradation by one of three accessory protein complexes: NEXT, TRAMP, or PAXT/PCC. NEXT is involved in turnover of introns released by pre-mRNA splicing and unstable RNAs from pervasive transcription. TRAMP degrades RNAs like pre-rRNAs, cryptic unstable transcripts, as well as a variety of aberrant small RNAs (tRNAs, ncRNAs, snoRNAs, snRNAs). PAXT/PCC is responsible for bringing nuclear ncRNAs with long polyA tails to the exosome. MTR4 is a member of the SKI2 family of RNA helicases that is common to all three nuclear exosome targeting complexes. To begin to implicate the exosome in regulation of *Neat1* and paraspeckles in macrophages, we transfected siRNAs designed against *Mtr4,* alongside a non-targeted control (NC), into RAW 264.7 macrophages. At 48 hours post-transfection, we achieved >90% knockdown of *Mtr4* (**Fig. S4A**). By RNA-FISH, we observed a dramatic increase in *Neat1* signal in resting *Mtr4* knockdown macrophages compared with NC siRNA control cells (**Fig. 4B**). This is consistent with reports of *Neat1* instability and a role for the exosome in controlling *Neat1* turnover (36). *Neat1* aggregates that form in the absence of MTR4 are *bona fide* structured PSs, as they each

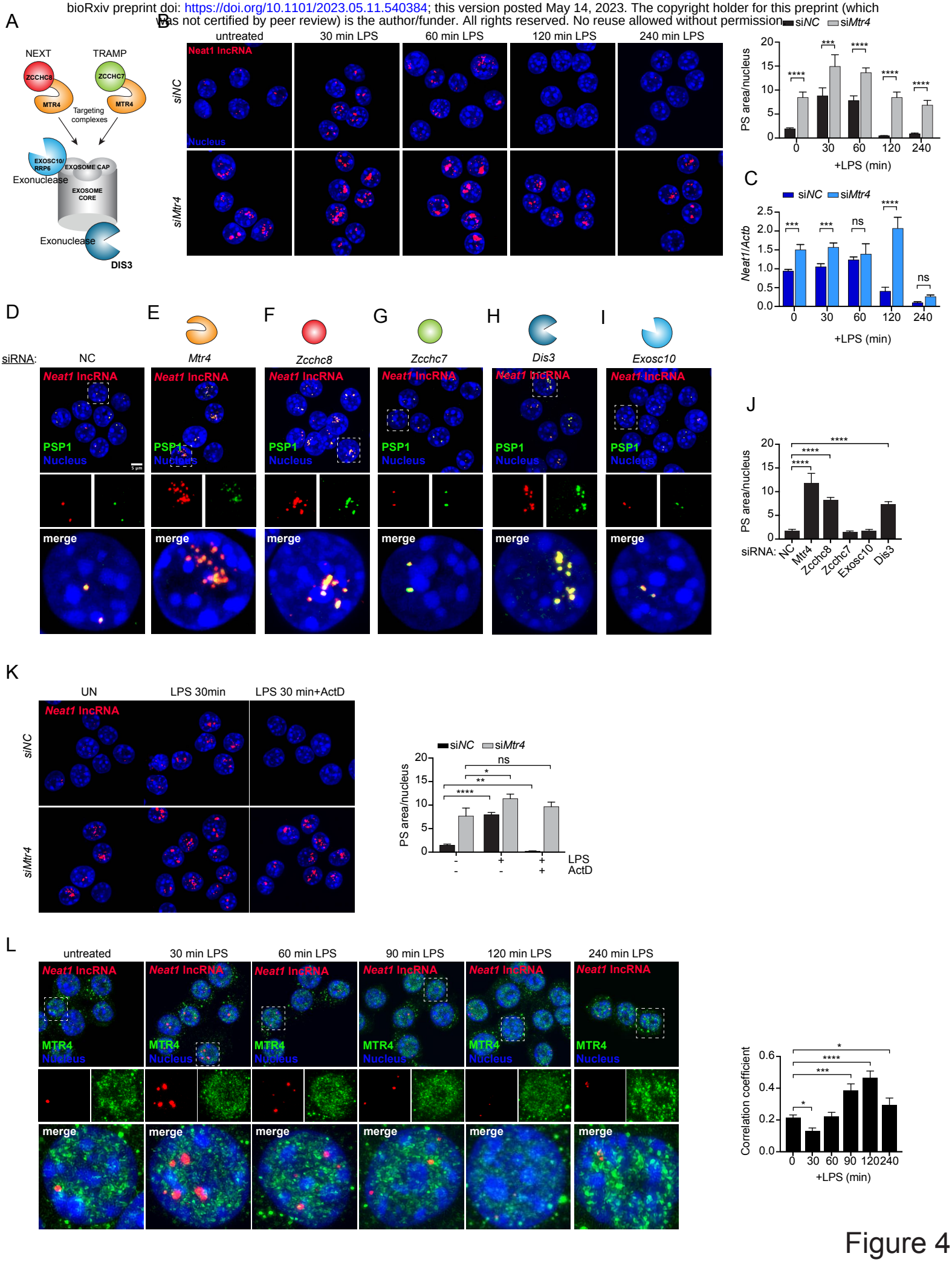

Figure 4

Figure 4: The NEXT complex targets the *Neat1* lncRNA to the nuclear exosome to regulate PS dynamics in macrophages.

(A) Model of nuclear RNA exosome and its three targeting complexes, NEXT, TRAMP, and PAXT. Colored shapes denote factors knocked down in 3D-I.
(B) RNA-FISH of *Neat1* (red) in *Mtr4* knockdown RAW 264.7 macrophages 48h after Silencer Select siRNA transfection, alongside a negative control siRNA, over a time-course of LPS treatment (100ng/ml). Quantitation of paraspeckle area/nucleus on right.
(C) RT-qPCR of *Neat1_2* transcript levels in siMtr4 and siNC RAW 264.7 macrophages after LPS treatment (100ng/ml) shown relative to *Actb.*
(D) RNA-FISH of *Neat1* (red) and immunofluorescence microscopy of PSP1 (green) in siNC RAW264.7 macrophages.
(E) As in (D), but in *siMtr4*-treated RAW 264.7 macrophages.
(F) As in (D), but in *siZcchc8*-treated macrophages.
(G) As in (D), but in *siZcchc7*-treated macrophages.
(H) As in (D), but in *siDis3*-treated macrophages
(I) As in (D), but in *siExosc10*-treated macrophages
(J) Quantitation of paraspeckle area/nucleus of 3D-I.
(K) RNA-FISH of *Neat1* (red) in *siNC* and *siMtr4*-treated RAW 264.7 macrophages in untreated cells, +LPS (100ng/ml; 30 min) or +ActD (5μg/ml; 30 min) followed by LPS (100ng/ml; 30 min).
(L) RNA-FISH of *Neat1* (red) and immunofluorescence microscopy of MTR4 (green) in RAW 264.7 macrophages after LPS treatment (100ng/ml). Quantitation of paraspeckle area/nucleus on right.
(J) FISH assay in RAW cells which were treated with siNC/siMTR4 for 48hrs and then treated with LPS alone or pre-treated with ActD for 30min and then treated with a 30 min LPS. Neat1: red, DAPI: blue. The cells were quantified for PS by Image J shown in the graph.

Statistical tests: Data is presented as the mean of three biological replicates unless otherwise noted with error bars representing SEM. At least 100 cells were counted over multiple coverslips per condition. Colocalization coefficient was measured using the ImageJ plugin Coloc2. Statistical significance was determined using a one-way ANOVA. *p<0.05, **p<0.01, ***p<0.001, ****p<0.0001.

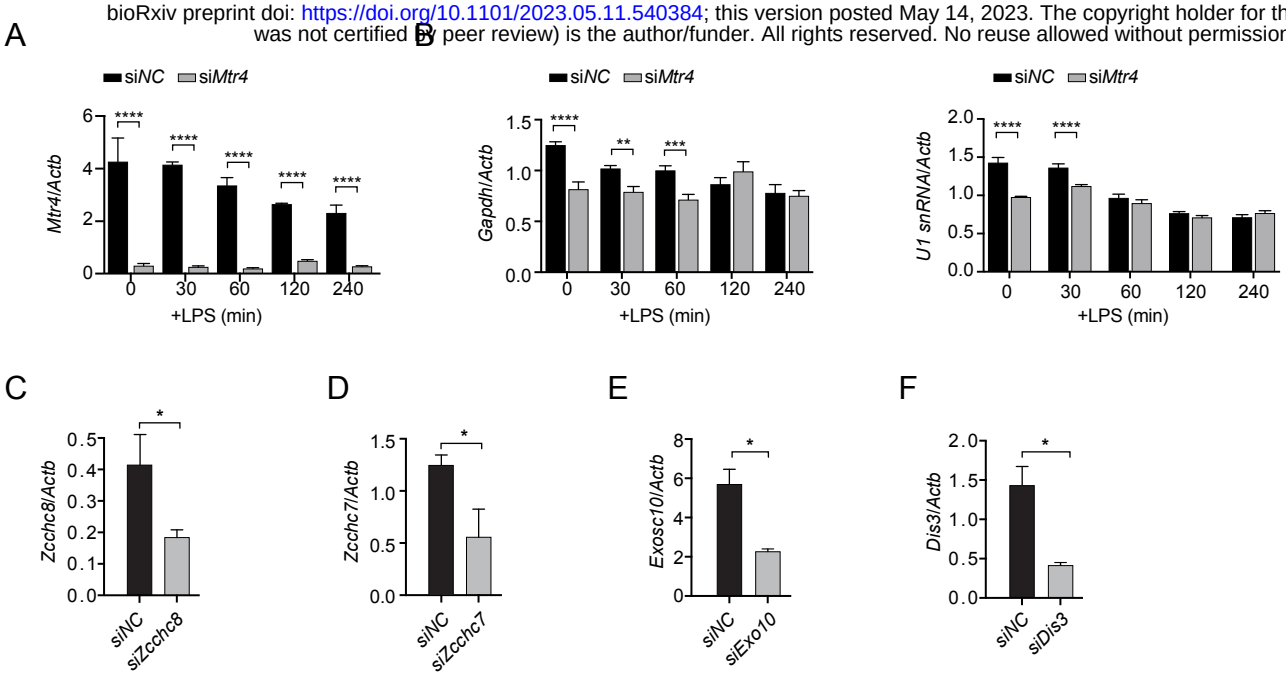

Figure S4

Figure S4: Supplementary Data for Figure 4

(A) RT-qPCR of *Mtr4* transcript levels in *siNC* and *siMtr4* RAW 264.7 macrophages over a time-course of LPS treatment (100 ng/ml), shown relative to *Actb*.
(B) As in (A) but for *Gapdh* and *U1 snRNA,* shown relative to *Actb*.
(C) RT-qPCR of *Zcchc8* transcript levels in *siNC* and *siZcchc8* RAW 264.7 macrophages, shown relative to *Actb*.
(D) As in (C) but for *Zcchc7* in *siNC* and *siZcchc7* RAW 264.7 macrophages
(E) As in (C) but for *Exosc10* in *siNC* and *siExosc10* RAW 264.7 macrophages
(F) As in (C) but for *Dis3* in *siNC* and *siDis3* RAW264.7 macrophages

Statistical tests: Data is presented as the mean of three biological replicates unless otherwise noted with error bars representing SEM. Statistical significance was determined using a one-way ANOVA. *p<0.05, **p<0.01, ***p<0.001, ****p<0.0001.

show significant enrichment with the paraspeckle protein PSP1 (**Fig. 4C-D**). Even though *Mtr4* KD macrophages have high numbers of paraspeckles at rest, these numbers still increase after LPS treatment (*siMtr4* time 0 vs. 30 and 60 minutes post-LPS; **Fig. 4B**). We interpret this to mean that aggregation of paraspeckles following LPS stimulation occurs independently of the exosome.

We can, however, implicate the exosome in paraspeckle disassembly at 120 minutes post-LPS. Notably, we do not see the characteristic loss of *Neat1* signal at 120 minutes post-LPS in *Mtr4* KD macrophages, implicating the exosome in controlling paraspeckle disintegration (**Fig 4B**). Surprisingly, while bulk measurements of *Neat1_2* cellular transcripts reflect this phenotype at 120 minutes (i.e. *Neat1* is higher in *siMtr4* relative to siNC cells), by 240 minutes, *Neat1_2* levels are very low regardless of whether cells have MTR4. This discrepancy at 240 minutes may stem from incomplete knockdown of *Mtr4,* where our bulk measurements read out some cells that have *Mtr4* knocked down and others that have normal levels of MTR4 (i.e. low levels of *Neat1*). It is also possible that some kind of transcriptional shut-off limits *Neat1* abundance even in exosome-knockdown cells. Regardless, we can conclude from these data that TLR4 engagement signals exosome-mediated dissolution of PS and turnover of *Neat1* at 120 minutes post-LPS treatment in macrophages.

Having implicated the MTR4 RNA exosome helicase in *Neat1* turnover and paraspeckle aggregation (**Fig. 4D-E, J**), we next sought to pin down the nature of the targeting complex and exonuclease that regulate *Neat1* stability in macrophages. Since *Neat1_2* is not polyadenylated, we ruled out a role for the PAXT/PCC targeting complex. To implicate either NEXT or TRAMP in *Neat1* turnover, we transfected RAW 264.7 macrophages with siRNAs directed against *Zcchc8* (NEXT) (**Fig. S4C**) and *Zcchc7* (TRAMP) (**Fig. S4D**) and observed paraspeckles (PSP1 and *Neat1*) by IF-FISH in resting cells. Loss of *Zcchc8* upregulated paraspeckles in a similar fashion to loss of *Mtr4* (**Fig. 4F, J**), while loss of *Zcchc7* had no impact on paraspeckle number or size (**Fig. 4G, J**). From this, we can conclude that *Neat1* is likely targeted to the exosome in macrophages by the NEXT complex. We performed a similar experiment to determine the exoribonuclease that degrades *Neat1*, comparing paraspeckles in resting *Exosc10* versus *Dis3* knockdown macrophages (**Fig. S4E-F**). We observed a clear upregulation of paraspeckles in cells transfected with siRNAs directed against *Dis3* but not *Exosc10* (**Fig. 4H-J**). Together, these data demonstrate that in resting macrophages, *Neat1* stability and paraspeckle maintenance is controlled by the NEXT targeting complex and the DIS3 exoribonuclease.

Next, we asked whether co-transcriptional PS assembly and exosome targeting of *Neat1* in macrophages are separable mechanisms. To do so, we treated *siNC-* and *siMtr4-transfected*

macrophages with LPS in the presence or absence of ActD, as in Fig. 3A. Whereas ActD completely ablated *Neat1* signal after 30 minutes in siNC cells (as we observed for wild-type macrophages in Fig. 3A), ActD had no impact on paraspeckles in *siMtr4* KD cells (**Fig. 4K**). Therefore, blocking the exosome allows for paraspeckle maintenance even in the absence of *de novo* transcription, suggesting a tug-of-war between transcription and exosome turnover in maintaining *Neat1* and paraspeckles in macrophages.

Lastly, we supposed that if *Neat1* is constitutively degraded by the exosome, as is suggested by the high number of paraspeckles we see in resting *Mtr4* knockdown macrophages (**Fig. 4B**), we might be able to detect co-localization between exosome components and the *Neat1* lncRNA. To test this, we performed FISH-IF using antibodies against MTR4. Indeed, we can detect colocalization between *Neat1* aggregates and MTR4 in resting cells, consistent with constitutive turnover of *Neat1* by the exosome. Moreover, over the course of LPS stimulation, we saw an inverse relationship between MTR4-*Neat1* colocalization and paraspeckle aggregation, whereby colocalization was lowest at 30 min, when paraspeckles are growing, and highest at 60-120 minutes when paraspeckles disintegrate (**Fig. 4L**). These data suggest a regulated mechanism of paraspeckle targeting to the exosome in macrophages and hint at undescribed links between pattern recognition receptor engagement and exosome activity.

Neat1 is required to activate the innate immune response in macrophages

Having observed dramatic, regulated reorganization of PSs in macrophages following LPS treatment, we finally asked whether ablating *Neat1*, and disrupting PS dynamics, impacted the macrophage innate immune response. To this end, we acquired mice that do not express *Neat1* due to incorporation of a lacZ cassette at the 5' end of the *Neat1* gene (37)(**Fig. S5A)**. Form these Neat1 KO mice, we differentiated BMDMs, treated them with LPS (10ng/ml) and isolated RNA for high-throughput sequencing and differential expression analysis at 2 hours and 4 hours post-stimulation. Loss of *Neat1* in these cells was confirmed by RNA-FISH (**Fig. 5A**). To enable identification of non-coding RNAs and incompletely processed RNAs whose abundance may be altered in the absence of *Neat1*, we generated our sequencing libraries using ribodepletion. Differential expression analysis uncovered hundreds of genes misregulated in *Neat1* KO macrophages ($log_2FC > 0.5, < -0.5$; adj. p-value <0.05) (208 genes at rest, 348 genes at 2h post-LPS, and 352 genes at 4h post-LPS) (**Fig. 5B**). We see about a third of the differentially expressed genes at each timepoint queried overlap (**Fig. S5B**), and using a hierarchical clustering algorithm, these genes breakdown into two discrete groups of upregulated and downregulated genes. We noted that many downregulated genes, especially those downregulated at 2

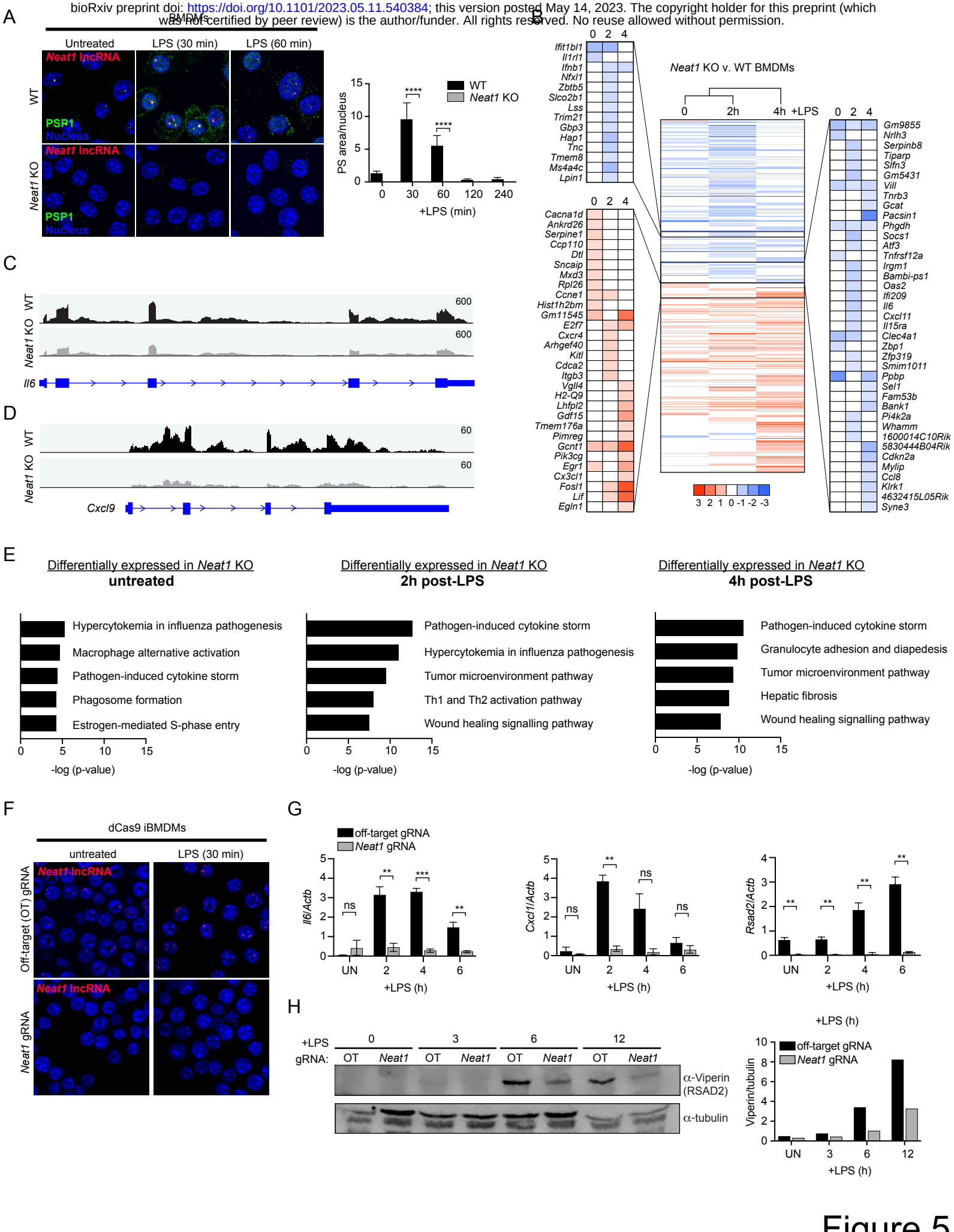

Figure 5

Figure 5: *Neat1* is required for proper up and downregulation of innate genes during the early macrophage response to LPS

(A) RNA-FISH of *Neat1* (red) and immunofluorescence microscopy of PSP1 (green) in WT and *Neat1* KO BMDMs over a 60 min time-course of LPS treatment (10ng/ml).
(B) Differential gene expression in *Neat1* KO v. WT BMDMs at 0, 2, and 4h post-LPS treatment. Genes were hierarchically clustered using Cluster 3.0 and visualized using Java TreeView. Clusters containing innate genes of interest shown as zoom-ins.
(C) Integrated Genomics Viewer tracks of RNA-seq reads from a representative WT and *Neat1* KO sample at the *Il6* genomic locus (mm10).
(D) As in (C) but for *Cxcl9*
(E) Ingenuity pathway analysis of pathways enriched for differentially expressed genes in Neat1 KO BMDMs v. WT at 0, 2, and 4h post-LPS stimulation (10ng/ml)
(F) RNA-FISH of *Neat1* (red) at 0 and 30 min post-LPS treatment (100ng/ml) of dCas9 iBMDMs transduced with an off-target (OT) gRNA lentiviral construct or a *Neat1* promoter-targeted gRNA lentiviral construct.
(G) RT-qPCR of *Il6*, *Cxcl1*, and *Rsad2* transcript levels in off-target gRNA and *Neat1* gRNA dCas9-expressing iBMDMs after LPS treatment (100ng/ml), shown relative to *Actb.*
(H) Immunoblot of Viperin (encoded by *Rsad2*) in off-target gRNA and *Neat1* gRNA dCas9-expressing iBMDMs after LPS treatment (100ng/ml). Quantitation, relative to tubulin, shown on right.

A

Adapted from Nakagawa et al. 2011

B

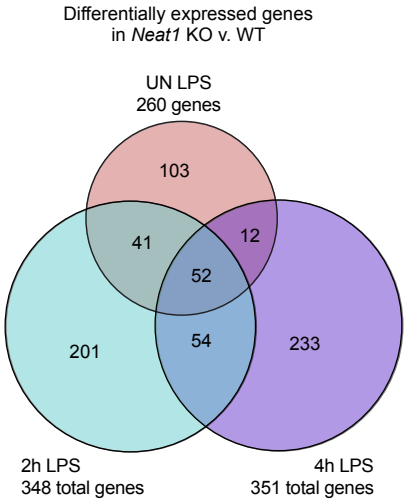

C

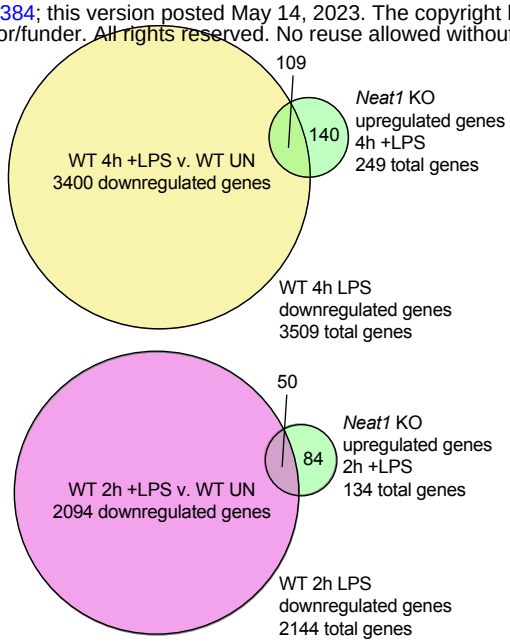

D

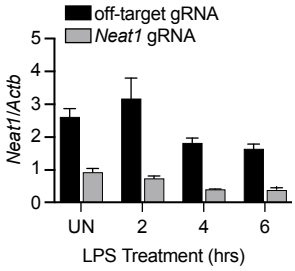

Figure S5

Figure S5: Supplementary Data for Figure 5

(A) Diagram of Neat1/lacZ (*Neat1* KO) mice
(B) Venn diagram of differentially expressed genes in *Neat1* KO v. WT BMDMs in untreated, 2h LPS-treated, and 4h LPS-treated macrophages.
(C) (top) Venn diagram of genes downregulated as part of the WT BMDM response to LPS (WT 4h+LPS v. WT UN; yellow) compared to genes upregulated at 4h +LPS in *Neat1* KO BMDMs (green). (bottom) Venn diagram of genes downregulated as part of the WT BMDM response to LPS (WT 2h+LPS v. WT UN; pink) compared to genes upregulated at 2h +LPS in *Neat1* KO BMDMs (green)
(D) RT-qPCR of *Neat1_2* transcript levels in off-target gRNA and *Neat1* gRNA-expressing dCas9 iBMDMs after LPS treatment (100ng/ml) shown relative to *Actb*.

and 4 hours post-LPS can be categorized as interferon stimulated genes (ISGs) (**Fig. 5B**). ISGs are induced downstream of cytosolic nucleic acid sensing, or TLR4 via the adapter TRIF, and are considered part of the macrophage antiviral response. Interestingly, many genes that we see upregulated in *Neat1* KO Macrophages (e.g *Cxcr4*, *Mxd3*, *Gdf15*; **Fig. 5B**) are normally downregulated as part of the wild-type macrophage response to LPS (**Fig. S5C**). These data suggest that *Neat1* KO macrophages fail to regulate macrophage gene expression in both directions—genes that are induced, cannot be fully induced and genes that are repressed cannot be fully repressed. Visualizing reads on the Integrated Genomics Viewer (Broad Institute), we observed differences in the abundance of reads aligning to both intronic and exonic sequences, suggesting that misregulation of innate gene expression in *Neat1* KO is not primarily driven by defects in splicing (**Fig. 5C, D**). Ingenuity Pathway Analysis identified several pathways enriched for genes that were differentially expressed in *Neat1* KO macrophages. Notably, *Neat1* KO macrophages show misregulation of inflammatory genes—particularly those with links to cytokine storms ("Pathogen-induced cytokine storm" and "Hypercytokemia in influenza pathogenesis"). We also observed defects in the ability of *Neat1* KO macrophages to express genes that control in macrophage polarization ("Macrophage alternative activation," "Th1 and Th2 activation pathway," and "Wound healing signaling pathway") (**Fig. 5E**). These data implicate *Neat1* in two critical aspects of macrophage biology: eliciting a balanced inflammatory response and differentiation into classical vs. alternative activation states.

As another strategy to eliminate *Neat1* from cells, we used lentiviral transduction to introduce a guide RNA directed against the *Neat1* promoter, alongside an untargeted control, into immortalized BMDMs expressing an endonuclease-deficient form of Cas9 (deactivated (dCas9)). We confirmed loss of *Neat1* expression in these CRISPRi (interference) cell lines by RT-qPCR and by *Neat1* RNA-FISH (**Fig. 5F**). Over a time-course of LPS treatment, we measured a dramatic defect in the ability of *Neat1* CRISPRi knockdown iBMDMs to induce expression of *Il6*, *Cxcl1,* and *Rsad2* (**Fig. 5G**), confirming that loss of *Neat1* results in a failure to induce innate genes in two different types of macrophages.

Lastly, we asked whether defects at the level of innate immune transcript accumulation are borne out at the protein level. Consistent with lower levels of *Rsad2* transcript, we measured less Viperin protein in *Neat1* gRNA dCas9 iBMDMs compared to OT gRNA control cells over a 12h LPS treatment (**Fig. 5H**). We then collected supernatants from WT and *Neat1* KO BMDMs and measured cytokine and chemokine secretion by multiplex cytokine array (Eve Technologies). We saw little evidence for differences in secretion of cytokines in resting *Neat1* KO and WT BMDMs (**Fig. S6A-J**). At 6h and 12h post-LPS treatment, we observed defects in both up

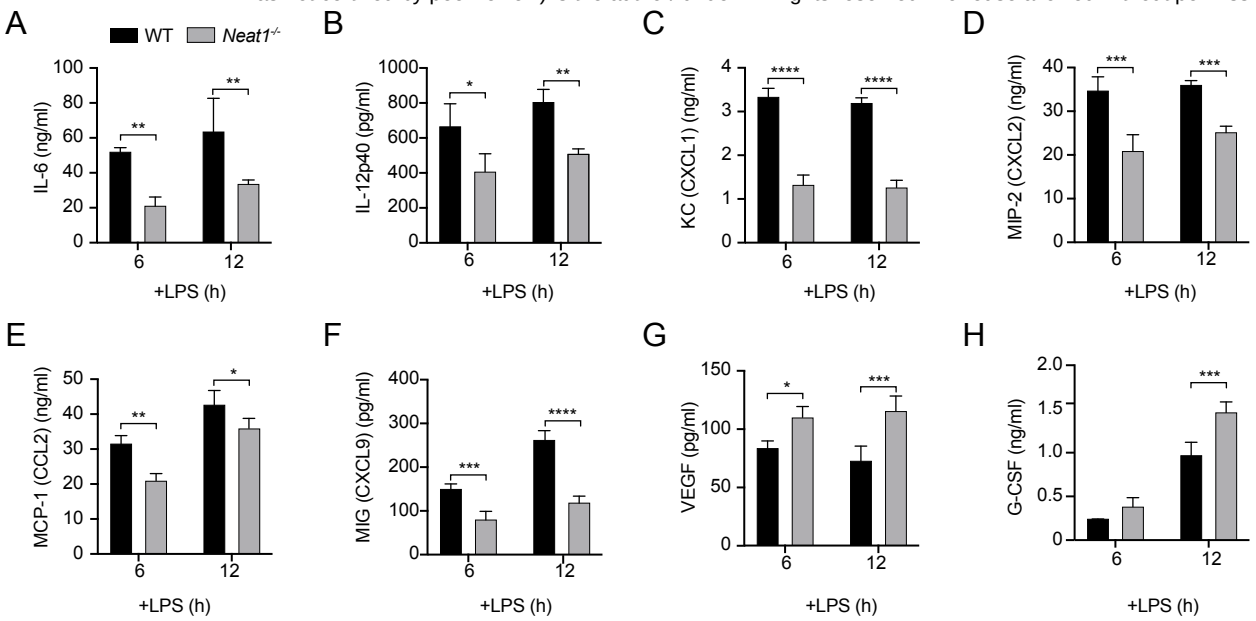

Figure 6

Figure 6: *Neat1* is required for proper cytokine and chemokine secretion in macrophages

(A) Measurements of IL-6 levels in the supernatants of WT and *Neat1* KO BMDM supernatants at 6 and 12h post-LPS treatment (10ng/ml) via cytokine array.
(B) As in (A) but for IL-12p40
(C) As in (A) but for KC (CXCL1)
(D) As in (A) but for MIP-2 (CXCL2)
(E) As in (A) but for MCP-1 (CCL2)
(F) As in (A) but for MIG (CXCL9)
(G) As in (A) but for VEGF
(H) As in (A) but for G-CSF

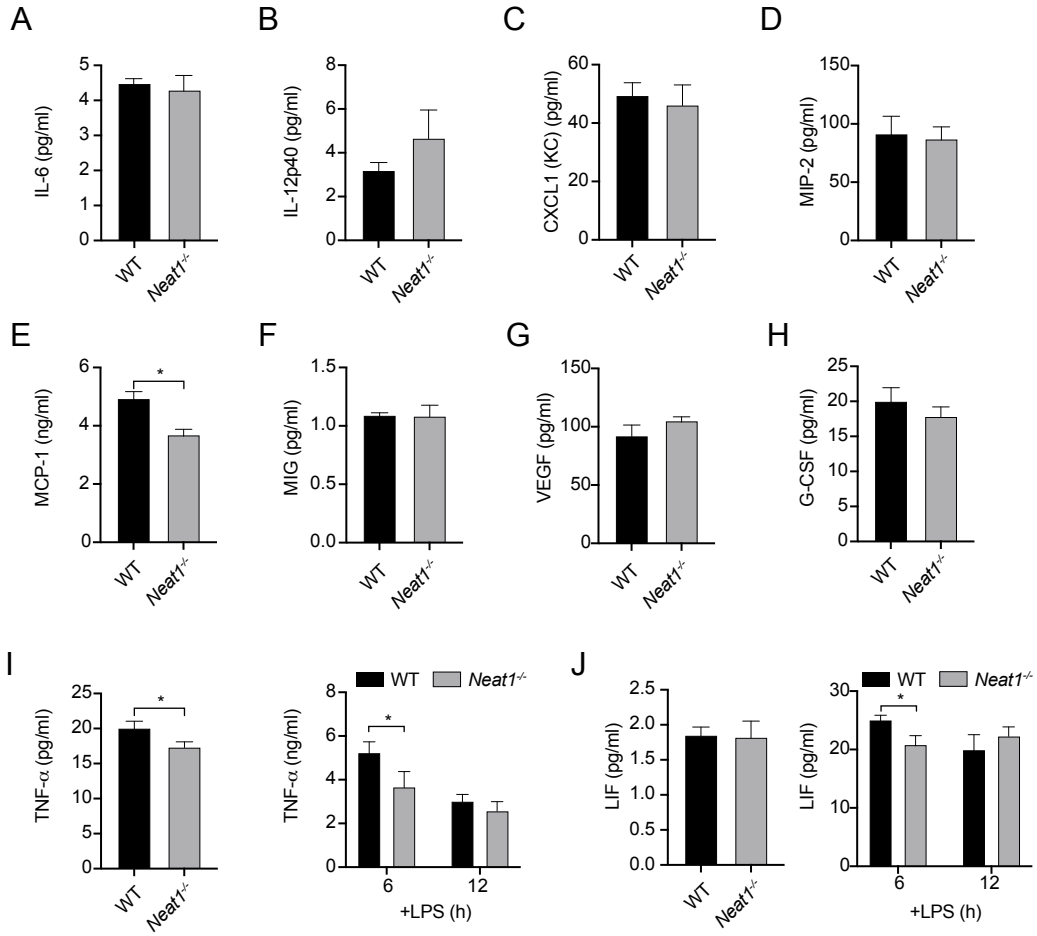

Figure S6

Figure S6: Supplementary Data for Figure 6

(A) Measurements of IL-6 levels in the supernatants of WT and *Neat1* KO BMDM supernatants at rest via cytokine array.
(B) As in (A) but for IL-12p40
(C) As in (A) but for KC (CXLC1)
(D) As in (B) but for MIP-2 (CXCL2)
(E) As in (A) but for MCP-1 (CCL2)
(F) As in (A) but for MIG (CXCL9)
(G) As in (A) but for VEGF
(H) As in (A) but for G-CSF
(I) Measurements of IL-6 levels in the supernatants of WT and *Neat1* KO BMDM supernatants at rest and at 6 and 12h post-LPS treatment via cytokine array.
(J) As in (I) but for LIF.

and downregulation of several cytokines at the level of protein synthesis/secretion in *Neat1* KO BMDMs. Cytokines and chemokines downregulated by loss of *Neat1*, such as IL-6, KC (aka CXCL1), MIP-2 (aka CXCL2), MCP-1 (aka CCL2), play critical roles in promoting inflammation and controlling infiltration of neutrophils and lymphocytes to sites of infection (**Fig. 6A-F**). Cytokines that are upregulated by loss of *Neat1*, such as VEGF (encoded by the *Vegfa* gene) and G-CSF (encoded by the *Csf3* gene), are involved in cell proliferation and differentiation (**Fig. 6G-H**). Our observation that soluble mediators of inflammation and infiltration are misregulated in macrophages lacking *Neat1* argues that the paraspeckle is needed to help macrophages establish a proper innate immune milieu *in vivo* in response to PAMP or DAMP sensing.

DISCUSSION

Despite enthusiasm surrounding the phenomenon of liquid-liquid phase separation and the structure of MLOs, the function of condensates in cellular homeostasis and stress responses remains poorly understood. Currently, our knowledge of paraspeckle structure and paraspeckle assembly far exceeds that of paraspeckle function. Here, we investigated a role for paraspeckles in activating the macrophage innate immune response following an infection-relevant stimulus (e.g. LPS). We report that paraspeckles rapidly aggregate, disassemble, and then re-form at steady state levels in a regulated fashion over a very short time-course (approximately 4 hours) in response to multiple innate agonists (**Fig. 1**). During this same time-course, we implicate paraspeckles and the *Neat1* lncRNA in promoting expression of a specific cohort of innate immune genes, including crucial pro-inflammatory cytokines and interferon stimulated genes following LPS stimulation (**Fig. 5-6**).

Based on these findings, we can conclude several things about the mechanism of paraspeckle assembly and disassembly in macrophages. Our data clearly demonstrate that maintenance and upregulation of paraspeckles in macrophages requires transcription: when ActD is added to macrophages, paraspeckles are no longer visible by RNA-FISH and no aggregation is seen upon LPS treatment (**Fig. 3**). As loading of paraspeckles proteins on *Neat1* has been shown to occur co-transcriptionally (22), we know that transcription of *Neat1* itself is needed for PS maintenance. However, whether *Neat1* itself is transcriptionally upregulated as part of the response to LPS remains unclear. By RT-qPCR, we typically measure a 2- to 3-fold increase in *Neat1* transcript levels at 60 minutes post-LPS treatment (**Fig. 1B**). This peak in total transcript is later than the peak of PS aggregation, which occurs at 30 min, suggesting that early PS aggregation is driven by sequestration of already synthesized *Neat1* as opposed to *de novo* transcription of new *Neat1* transcripts. This makes sense, given the rapid aggregation of

PS observed (15-30 minutes) and the length of *Neat1* itself (21.1 kb), which will take some time to fully transcribe. Previously published RNA sequencing data and ChIP-seq data for the NFκB transcription factor subunit RelA (38) show some evidence for RelA binding at the *Neat1* promoter following LPS stimulation of BMDMs (**Fig. S3D**), although this was not concomitant with significantly increased *Neat1* sequencing reads (**Fig. S3E**). Together, these data and our findings support a model whereby paraspeckle aggregation in macrophages does not require cells to make more *Neat1*, although it is possible that bulk measures of *Neat1* RNA from a population of cells is obscuring our ability to accurately measure *Neat1* transcriptional activation. Promoter fusion constructs and/or single cell transcriptomics may help answer the question of whether *Neat1* is induced downstream of pattern recognition receptor engagement and help reconcile our findings with other studies whose models invoke *Neat1* transcriptional upregulation following PAMP sensing in non-immune cells (19).

We can also conclude that the RNA exosome, specifically the NEXT targeting complex, is involved in turning over *Neat1* and regulating paraspeckle dynamics in macrophages (**Fig. 4**). This is consistent with another report linking MTR4 and NEXT to *Neat1* turnover, although the kinetics of *Neat1* turnover reported in HeLa cells (loss of detectable *Neat1* transcript by 6-8 hours post-transcription shut-off) are different from what we see in macrophages (2 hours) (39). The fact that we see paraspeckle upregulation in resting *Mtr4*, *Zcchc8*, and *Dis3* knockdown macrophages demonstrates a role for the exosome in constitutively controlling paraspeckle size/numbers. The fact that we see paraspeckles maintained in exosome knockdown macrophages even at timepoints when paraspeckles disaggregate in wild-type cells (120 minutes post-LPS) can mean two things: 1.) exosome targeting of *Neat1* is enhanced at 120 minutes post-LPS treatment, suggesting that the exosome itself is regulated downstream of pattern recognition receptor engagement or 2.) exosome turnover of *Neat1* is constant and *Neat1* transcription is turned off in a regulated fashion. Potential mechanisms for such a turn off could include competition between the long and short isoforms of *Neat1*, histone modification/chromatin remodeling at the *Neat1* promoter, and altered association of the *Neat1* genomic locus with enhancer elements. Again, promoter fusions and/or cell lines that enable rapid loss of exosome components (like the auxin degron system in (40)) could help tease apart the role of transcription versus turnover in regulating *Neat1* levels post-LPS treatment.

One curious observation made regarding paraspeckles in macrophages is their apparent lack of enrichment for several proteins reported to be essential paraspeckle components in model cell types, like NIH3T3s (10). For example, at no point in the macrophage paraspeckle "lifecycle" do we observe paraspeckle-like puncta for FUS or BRG1 (**Fig. S2B-C**). Both of these

essential paraspeckle factors displaying diffuse nuclear staining in the presence and absence of LPS in macrophages, suggesting that the composition of the paraspeckle is cell-type specific. While our macrophage data seemingly calls for a redefinition of the requirements for paraspeckle assembly, it is possible like FUS and BRG1 can control condensation of the particle without being part of its structure. Consequently, future experiments designed to define the PS proteome will not only inform on what proteins are moved in and out of the PS following macrophage activation, but also provide insight into the potentially unique composition of the resting macrophage paraspeckle.

Another curiosity of the macrophage paraspeckle is its disintegration at 2 hours post-LPS treatment. To the best of our knowledge, this is the first report of paraspeckle ablation following a physiologically relevant cellular stress. At 2 hours post-LPS treatment, the macrophage innate response is still ramping up, with maximum transcript accumulation for many inflammatory and antimicrobial genes seen at 4-6h post-stimulation. Breakdown of paraspeckles at 2 hours post-LPS could aid in this amplification by releasing factors involved in nucleosome remodeling at secondary response genes (e.g., SWI/SNF components (29)) or post-transcriptional processing of innate transcripts (e.g., RBPs). Such a model would make PS disintegration a critical step in activation of inflammatory responses and may position the PS as a stopgap to prevent this “ramping up” (i.e., continue to sequester innate activating proteins) in the absence of a strong stimulus. On the other hand, it is possible that early PS aggregation sequesters inhibitory factors to help activate the innate response. Such a model has been proposed for relief of SFPQ repression of *IL8* transcription in HeLa cells (19). Consistent with this idea, we observed increased colocalization between the RNA binding protein hnRNP M and *Neat1* following LPS treatment (**Fig. 2D**). Our previous work showed that hnRNP M can repress innate gene expression in macrophages by slowing intron removal in inflammatory transcripts like *Il6* (28). Thus, is it possible that dampened IL-6 expression in *Neat1* KO macrophages is driven in part by failure to sequester hnRNP M from nascent pre-mRNAs. Sequestration of hnRNP M, however, is likely not the only RBP regulated by the macrophage PS that could impact innate immune gene expression. Indeed, the dual action of *Neat1* in promoting expression of genes turned on by LPS and dampening expression of genes turned off by LPS suggests a complex role for the PS in activating and repressing innate gene expression through sequestration of RBPs with diverse functions. While we do not fully understand the molecular mechanisms driving these phenomena, we can conclude that the nuclear paraspeckle plays a crucial and underappreciated role in globally regulating the macrophage innate response to pathogens.

ACKNOWLEDGEMENTS

The authors would like to thank members of the Patrick and Watson labs for helpful discussions and manuscript edits. Our sincerest appreciation goes to Malea Murphy and the Integrated Microscopy and Imaging Laboratory (IMIL) at Texas A&M University School of Medicine, who helped with acquisition and analysis of our FISH-IF images. We would also like to acknowledge the Genomics and RNA Profiling Core at Baylor College of Medicine for library generation and high-throughput sequencing and the CRISPR Core at the University of California, Santa Cruz (RRID:SCR_021207) for generating gRNA-expressing lentivirus.

MATERIALS AND METHODS

RNA FISH and immunofluorescence microscopy

Fluorescence In Situ Hybridization-Immunofluorescence (FISH-IF) was used to simultaneously visualize RNA and protein. Briefly, 1 x 10^5 RAW 264.7 macrophages or BMDMS were plated in a glass bottom 35mm Mattek dish and allowed to rest for 24h. Cells were washed with 1xPBS and fixed with 4% paraformaldehyde for 10 minutes, and then washed 3x with 1xPBS. Cells were permeabilized with 0.5% Triton X-100 for 10 minutes, washed twice with PBS and once with 2xSSC buffer (Sigma, S6639) for 10 minutes. Cells were incubated overnight with probes in hybridization buffer (1:200). A pool of 48 *Neat1* smFISH (single molecule Fluorescence In-Situ Hybridization-Immunofluorescence) RNA probes were designed and purchased from Stellaris® (SMF-3010-1, Mouse *Neat1* Middle Segment with Quasar® 570 Dye). Following probe incubation, cells were washed with 2xSSC each time for 15 minutes, and then 3 times with PBS. DAPI (Invitrogen, D1306, 1:10,000) was used for 10 minutes for nuclear staining, followed by four PBS washes for 5 minutes each. For immunofluorescence, primary antibodies (1:200) against SFPQ (Abcam, ab177149), PSP1 (Abcam, ab214012), NONO (Abcam, ab133574), HNRNP M (Abcam, ab177957), FUS (Abcam, ab243880), BRM (Abcam, ab240648), BRG1 (Abcam, ab110641), NF-κB (Active Motif, Catalog No: 40916) were used along with 10% BSA (NEB #B9200) as a blocking agent. Cells were overnight incubated with primary antibody at 4°C, and then washed with PBS three times for 5 minutes each. Cells were then stained with fluorescent secondary antibodies (goat anti-rabbit Alexa Fluor 488, and/or goat anti-mouse Alexa Fluor 488; Invitrogen, 1:1,000), and finally washed with PBS three times for 5 minutes each. Images were taken on an Olympus Fluoview FV3000 confocal laser scanning microscope using the 60X objective and processed and analyzed with Fiji.

Primary Cell Culture

To prepare primary cell cultures of bone marrow-derived macrophages (BMDMs), bone marrow (BM) cells were isolated from mouse femurs by washing them with 10 mL DMEM 1 mM sodium pyruvate (ThermoFisher, 11995065), followed by centrifugation for 5 minutes at 400 RCF and resuspension in BMDM media consisting of Dulbecco modified Eagle medium (DMEM), 20% of heat-inactivated fetal bovine serum (FBS) (Millipore, F0926), 1 mM sodium pyruvate (Lonza, BE13-115E), and 10% MCSF conditioned media. BM cells were counted and seeded at a density of 5x10^6 cells per 15 cm non tissue culture-treated dish in 30 ml complete BMDM media. An

additional 15 mL of BMDM media was added on day 3, and cells were harvested on day 7 using 1 X PBS EDTA (Lonza, BE02-017F) for experiments.

Cell Lines and Cell Culture

Low passage stocks of RAW 264.7 macrophages were obtained from ATCC (TIB-71), were cultured at 37°C/5% CO2 in complete media containing high glucose DMEM (Thermo Fisher, 11965092), with 10% FBS (Millipore, F0926) and 0.2% HEPES (Thermo Fisher, 15630080). Cells were harvested using 1xPBS + EDTA or cell scraper. Absence of mycoplasma was confirmed in all cell lines using the Universal Mycoplasma Detection Kit (ATTC, 30–1012 K). dCas9 iBMDMs obtained from the Carpenter Lab at University of California, Santa Cruz (UCSC), were cultured at 37°C/5% CO_2 in complete media containing high glucose DMEM (Thermo Fisher, 11965092), with 10% FBS (Millipore, F0926) and 0.2% HEPES (Thermo Fisher, 15630080). To make *Neat1* gRNA-expressing cell lines, 2.5 x 10^4 cells were plated in a 24-well treated tissue culture plate and incubated for 24hrs. The cells were then transduced with *Neat1* gRNA or off-target gRNA lentivirus generated by the UCSC CRISPR Core in the presence of 0.5 μl lipofectamine 2000 (Thermo Fisher, 52887). Twenty-four hours after initial transduction, lentivirus was removed and replaced with complete media containing high glucose DMEM for another 24hrs. 48h post-transduction, cells were selected via the addition of 3μg/mL puromycin (Invivogen, ant-pr-1). 96hrs post-transduction, cells were selected in final concentration of 5μg/mL puromycin and maintained in this concentration of drug.

Cell Stimulations and Treatments

BMDMs/RAW 264.7 macrophages were plated at 5 x 10^5 cells/well in 12-well dishes. For FISH and IF-FISH, 1 x 10^5 cells were plated into 35mm Mattek plates a day prior to stimulation. LPS stimulations were done with 100 ng/ml LPS (InvivoGen) for RAW 264.7 macrophages and 10ng/ml LPS for BMDMs for times indicated. Cells were treated with 100 ng/ml Pam3CSK4 (InvivoGen) or transfected with 1 μg/ml ISD, or 500 ng/ml poly(I:C) using lipofectamine (Thermo Fisher). For transcription inhibition, 5x10^5 cells/well were plated in a 12-well dish or 35mm Mattek plates and transcription was blocked by using 5 μg/ml actinomycin D for 30min. For kinase inhibitor experiments, cells were plated in 35mm Mattek/12-well plates and treated with P38 inhibitor (SB203580) 10 μM, MEK1/2 Inhibitor (U0126) 25 μM or JNK inhibitor (SP600125) 25 μM, (InvivoGen) for 45 minutes prior to imaging.

To polarize RAW 264.7 macrophages into M1/M2 macrophages, RAW 264.7 macrophages were plated in a glass bottom 35mm Mattek (P35G-1.5-14-C) or 12 well plates and treated with 50 ng/mL of IFN-γ (R & D, 485-MI) or 25 ng/mL of IL-4 (PeproTech, 214-14) for 24 hours. Macrophages polarization was confirmed by gene expression analysis.

siRNA Transfections

To perform mRNA knockdown of exosome components, cells were plated in 12-well plates at a density of 3 x 10^5 RAW 264.7 macrophages or 3.5 x 10^5 BMDMs on day 4 of differentiation and rested overnight. The next day, complete media was replaced with 500 µL fresh complete media 30 minutes prior to transfection. Transfection was carried out using Fugene SI reagent (SKU:SI-100) along with 50µM of ThermoFisher siRNA stock against Skiv2l2 (Mtr4); s90745), Zcchc8; s89034, Zcchc7; s38623, Dis3; s91196, and Exosc10; s78572). For a negative control, Silencer Select Negative Control #1 (ThermoFisher, 4390843) was used. Cells were incubated for 48h in transfection media at 37°C with 5% CO_2 before conducting downstream experiments.

***Neat1* KO Mice genotyping**

Neat1 KO mice used in this study were obtained from the laboratory of Shinichi Nakagawa at Hokkaido University (37). Briefly, a BAC clone RP23-209P9 was used as a template to amplify DNA fragments through PCR, which were subsequently subcloned into DT-ApA/LacZ/NeO to create the targeting vector. Homologous recombination was verified through Southern blot analysis after electroporation of the linearized targeting vector into TT2 embryonic stem cells. Chimeric mice were produced using the recombinant embryonic stem clone and crossed with C57BL/6 females to generate NEAT1lacZ/Neo/+ heterozygous animals. These mice were then bred with Gt (ROSA) 26 Sortm1 (FLP1) Dym (The Jackson Laboratory) to flip out the PGK-Neo cassette. The resulting heterozygous mice (NEAT1 lacZ/+) were maintained on the C57BL/6 genetic background and genotyped through PCR using DNA obtained from ear clips. The genotyping primer sequences are NEAT1 WT FW: CTAGTGGTGGGGAGGCAGT, NEAT1 WT RV: AGCAGGGATAGCCTGGTCTT, LacZ 5(KO) RV: GCCATTCAGGCTGCGCAACTG. The mice used in our experiments were age- and sex-matched controls, with 8-12 week old mice used to generate BMDMs. All mice were housed, bred, and studied at Texas A&M Health Science Center in accordance with approved Institutional Care and Use Committee guidelines.

RNA Sequencing

RNA from *Neat1*$^{-/-}$ and WT BMDMs was isolated using TRIzol. Ribodepletion library preparation was carried out by the Baylor College of Medicine Genomic and RNA Profiling Core (GARP) in biological triplicate. RNA sequencing (150bp paired-end reads) was performed on an Illumina NovaSeq 6000 with S4 flow cell. STAR alignment to the *Mus musculus* Reference genome (mm10) and differential expression analysis was carried out using Illumina BaseSpace RNA-Seq Alignment and RNA-seq Differential Expression apps. Differentially expressed genes were identified based on an adj. p-value threshold of <0.05 and a $\log_2$FC of +/- 0.5. For transcriptome analysis, Qiagen IPA analysis was utilized to generate lists of GO terms and disease pathways.

Immunoblot

Cells were washed with PBS and lysed in 1X RIPA buffer with protease and Pierce EDTA free phosphatase inhibitors (Thermo Scientific, A32957) with 1 U/mL of benzonase nuclease (Millipore, 101697) added to degrade genomic DNA. Proteins were separated by SDS-PAGE on Any kD mini-PROTEAN TGX precast gel (BioRad) and transferred to 0.45 µm nitrocellulose membranes (Cytiva, 10600041). After blocking the membranes for 1 hour at RT in LiCOR Odyssey blocking buffer (927-60001), they were incubated overnight at 4°C with the relevant primary antibodies, including β-ACTIN (Abcam 6276, 1:5000), SFPQ (ab177149, 1:1000), PSP1 (ab214012, 1:1000), NONO (ab133574, 1:1000), Anti-phosphoepitope SR proteins, clone 1H4 (EMD Millipore, MABE50, 1:1000). Membranes were washed three times for 5 minutes in PBS-Tween-20 and incubated with the appropriate secondary antibodies (LI-COR, 925-32210, 926-68071) for 1 hour at RT before imaging on a LiCOR Odyssey Fc Dual-Mode Imaging System.

RNA Isolation and RT-qPCR Analysis

RNA was isolated from cells harvested in TRIzol using Direct-zol RNA Miniprep kits (Zymo Research, R2052) with an hour DNase treatment. cDNA was synthesized using iScript cDNA Synthesis Kit (Bio-Rad, 1708891) and diluted to 1:20 for each sample. A standard curve was generated using a pool of cDNA from each treated sample. RT-qPCR was performed using Power-Up SYBR Green Master Mix (Thermo Fisher, A25742) and a QuantStudio Flex6 (Applied Biosystems) with triplicate wells in a 384-well plate.

Data Analysis and Presentation

Graphpad Prism software (Version 9) was used to perform statistical analysis of data and generate graphs. Unless otherwise indicated, the results presented are from at least three biological samples and are represented as the mean, with error bars representing SEM. We used a t test

and one/two-way analysis of variance (ANOVA) to determine significant differences between the means of the control groups versus experimental groups. Quantification of PS area was carried out by measuring the 3D area of signal in ≥100 cells using Fiji software. RNA and protein co-localization was analyzed using the Coloc 2 plugin in Fiji (ImageJ) software. Briefly, the images were first background-subtracted and thresholded to generate binary masks of the *Neat1* RNA and protein signals. The Pearson correlation coefficient, a quantitative measure of the degree of co-localization between the two signals, was then calculated and graphed.

Primers

Sequences of the primer sets used in this paper are as follows:
Neat1-V2-Fwd: GTGGTCTCTGTGGAAGTGTATG
Neat1-V2-Rev: TGGAGAAGCGAAACGAGATG,
TNF-Fwd: CCGATGGGTTGTACCTTGTC
TNF-Rev: AGATAGCAAATCGGCTGACG
lL-1B-Fwd: GGTGTGTGACGTTCCCATTA
lL-1B-Rev: ATTGAGGTGGAGAGCTTTCAG
Malat1-Fwd: GATGACTCAAGGGAACCAGAAA
Malat1-Rev: GAAAGCTAGCATCCATCCTCT AC
Nos2-Fwd: GCAGCACTTGGATCAGGAA
Nos2-Rev: GAAACTTCGGAAGGGAGCAA
GAPDH-Fwd: CAATGTGTCCGTCGTGGATCT
GAPDH -Rev: GTCCTCAGTGTAGCCCAA GAT
Kcnq1ot1-Fwd: CGTTATCCAGACTCTCCCTTTC
Kcnq1ot1-Rev: GTTACCTCTTTCAGGGCT TCT
MTR4-Fwd: CCCACTCCACAATGATCCTAAC
MTR4-Rev: CTTGCCTTCTTCAGTTCTCTCTT
Dis3-Fwd: ACACACATTTCACCTCTCCTATC
Dis3-Rev: GTCAACTCAGGGTAAGTACAGTC
Exosc10-Fwd: CTGTTTGCTTGGAGGGATAAGA
Exosc10-Rev: GGCAGTTCCTCAGCTATCTTTAG
Zcchc7-Fwd: GGAGGAGAGGACATAGCAAATAC
Zcchc7-Rev: CAAGTTTGAGGATGCCTTTCAC
ZCCHC8-Fwd: GCTTACGGAAGGATGGGAAATA
ZCCHC8-Rev: CAGTTGAAACAGTGAGGCTTTG

REFERENCES

1. E. M. Courchaine, A. Lu, K. M. Neugebauer, Droplet organelles? *EMBO J* **35**, 1603-1612 (2016).
2. H. Ismail *et al.*, Mechanisms and regulation underlying membraneless organelle plasticity control. *J Mol Cell Biol* **13**, 239-258 (2021).
3. C. S. Bond, A. H. Fox, Paraspeckles: nuclear bodies built on long noncoding RNA. *J Cell Biol* **186**, 637-644 (2009).
4. A. H. Fox *et al.*, Paraspeckles: a novel nuclear domain. *Curr Biol* **12**, 13-25 (2002).
5. J. A. West *et al.*, Structural, super-resolution microscopy analysis of paraspeckle nuclear body organization. *J Cell Biol* **214**, 817-830 (2016).
6. A. H. Fox, C. S. Bond, A. I. Lamond, P54nrb forms a heterodimer with PSP1 that localizes to paraspeckles in an RNA-dependent manner. *Mol Biol Cell* **16**, 5304-5315 (2005).
7. A. H. Fox, S. Nakagawa, T. Hirose, C. S. Bond, Paraspeckles: Where Long Noncoding RNA Meets Phase Separation. *Trends Biochem Sci* **43**, 124-135 (2018).
8. T. Yamazaki *et al.*, Functional Domains of NEAT1 Architectural lncRNA Induce Paraspeckle Assembly through Phase Separation. *Mol Cell* **70**, 1038-1053 e1037 (2018).
9. E. Gomes, J. Shorter, The molecular language of membraneless organelles. *J Biol Chem* **294**, 7115-7127 (2019).
10. T. Naganuma *et al.*, Alternative 3'-end processing of long noncoding RNA initiates construction of nuclear paraspeckles. *EMBO J* **31**, 4020-4034 (2012).
11. Y. T. Sasaki, T. Ideue, M. Sano, T. Mituyama, T. Hirose, MENepsilon/beta noncoding RNAs are essential for structural integrity of nuclear paraspeckles. *Proc Natl Acad Sci U S A* **106**, 2525-2530 (2009).
12. C. M. Clemson *et al.*, An architectural role for a nuclear noncoding RNA: NEAT1 RNA is essential for the structure of paraspeckles. *Mol Cell* **33**, 717-726 (2009).
13. T. Hirose *et al.*, NEAT1 long noncoding RNA regulates transcription via protein sequestration within subnuclear bodies. *Mol Biol Cell* **25**, 169-183 (2014).
14. M. Modic *et al.*, Cross-Regulation between TDP-43 and Paraspeckles Promotes Pluripotency-Differentiation Transition. *Mol Cell* **74**, 951-965 e913 (2019).
15. D. Reddy *et al.*, Paraspeckles interact with SWI/SNF subunit ARID1B to regulate transcription and splicing. *EMBO Rep* **24**, e55345 (2023).
16. W. van Leeuwen, C. Rabouille, Cellular stress leads to the formation of membraneless stress assemblies in eukaryotic cells. *Traffic* **20**, 623-638 (2019).
17. C. Wang *et al.*, Stress Induces Dynamic, Cytotoxicity-Antagonizing TDP-43 Nuclear Bodies via Paraspeckle LncRNA NEAT1-Mediated Liquid-Liquid Phase Separation. *Mol Cell* **79**, 443-458 e447 (2020).
18. P. Zhang, L. Cao, R. Zhou, X. Yang, M. Wu, The lncRNA Neat1 promotes activation of inflammasomes in macrophages. *Nat Commun* **10**, 1495 (2019).
19. K. Imamura *et al.*, Long Noncoding RNA NEAT1-Dependent SFPQ Relocation from Promoter Region to Paraspeckle Mediates IL8 Expression upon Immune Stimuli. *Mol Cell* **54**, 1055 (2014).
20. J. Saini, U. Thapa, B. Bandyopadhyay, S. Vrati, A. Banerjee, Knockdown of NEAT1 restricts dengue virus replication by augmenting interferon alpha-inducible protein 27 via the RIG-I pathway. *J Gen Virol* **104** (2023).
21. T. Naganuma, T. Hirose, Paraspeckle formation during the biogenesis of long non-coding RNAs. *RNA Biol* **10**, 456-461 (2013).

22. Y. S. Mao, H. Sunwoo, B. Zhang, D. L. Spector, Direct visualization of the co-transcriptional assembly of a nuclear body by noncoding RNAs. *Nat Cell Biol* **13**, 95-101 (2011).
23. Y. Beeharry, G. Goodrum, C. J. Imperiale, M. Pelchat, The Hepatitis Delta Virus accumulation requires paraspeckle components and affects NEAT1 level and PSP1 localization. *Sci Rep* **8**, 6031 (2018).
24. K. Imamura *et al.*, Long noncoding RNA NEAT1-dependent SFPQ relocation from promoter region to paraspeckle mediates IL8 expression upon immune stimuli. *Mol Cell* **53**, 393-406 (2014).
25. P. J. Murray, Macrophage Polarization. *Annu Rev Physiol* **79**, 541-566 (2017).
26. T. Hirose, T. Yamazaki, S. Nakagawa, Molecular anatomy of the architectural NEAT1 noncoding RNA: The domains, interactors, and biogenesis pathway required to build phase-separated nuclear paraspeckles. *Wiley Interdiscip Rev RNA* **10**, e1545 (2019).
27. H. An, J. T. Tan, T. A. Shelkovnikova, Stress granules regulate stress-induced paraspeckle assembly. *J Cell Biol* **218**, 4127-4140 (2019).
28. K. O. West *et al.*, The Splicing Factor hnRNP M Is a Critical Regulator of Innate Immune Gene Expression in Macrophages. *Cell Rep* **29**, 1594-1609 e1595 (2019).
29. V. R. Ramirez-Carrozzi *et al.*, Selective and antagonistic functions of SWI/SNF and Mi-2beta nucleosome remodeling complexes during an inflammatory response. *Genes Dev* **20**, 282-296 (2006).
30. M. B. Clark *et al.*, Genome-wide analysis of long noncoding RNA stability. *Genome Res* **22**, 885-898 (2012).
31. D. Strassheim *et al.*, Phosphoinositide 3-kinase and Akt occupy central roles in inflammatory responses of Toll-like receptor 2-stimulated neutrophils. *J Immunol* **172**, 5727-5733 (2004).
32. T. Kawai, S. Akira, Signaling to NF-kappaB by Toll-like receptors. *Trends Mol Med* **13**, 460-469 (2007).
33. B. E. Aubol *et al.*, N-terminus of the protein kinase CLK1 induces SR protein hyperphosphorylation. *Biochem J* **462**, 143-152 (2014).
34. J. Prasad, J. L. Manley, Regulation and substrate specificity of the SR protein kinase Clk/Sty. *Mol Cell Biol* **23**, 4139-4149 (2003).
35. J. Houseley, J. LaCava, D. Tollervey, RNA-quality control by the exosome. *Nat Rev Mol Cell Biol* **7**, 529-539 (2006).
36. T. Tanu *et al.*, hnRNPH1-MTR4 complex-mediated regulation of NEAT1v2 stability is critical for IL8 expression. *RNA Biol* **18**, 537-547 (2021).
37. S. Nakagawa, T. Naganuma, G. Shioi, T. Hirose, Paraspeckles are subpopulation-specific nuclear bodies that are not essential in mice. *J Cell Biol* **193**, 31-39 (2011).
38. A. J. Tong *et al.*, A Stringent Systems Approach Uncovers Gene-Specific Mechanisms Regulating Inflammation. *Cell* **165**, 165-179 (2016).
39. K. Imamura *et al.*, Diminished nuclear RNA decay upon Salmonella infection upregulates antibacterial noncoding RNAs. *EMBO J* **37** (2018).
40. L. Davidson *et al.*, Rapid Depletion of DIS3, EXOSC10, or XRN2 Reveals the Immediate Impact of Exoribonucleolysis on Nuclear RNA Metabolism and Transcriptional Control. *Cell Rep* **26**, 2779-2791 e2775 (2019).